




REPORT

The LTB₄–BLT1 axis regulates actomyosin and β₂-integrin dynamics during neutrophil extravasation

Bhagawat C. Subramanian¹, Nicolas Melis¹, Desu Chen¹, Weiye Wang¹, Deborah Gallardo², Roberto Weigert^{1*}, and Carole A. Parent^{1,3*}

The eicosanoid leukotriene B₄ (LTB₄) relays chemotactic signals to direct neutrophil migration to inflamed sites through its receptor BLT1. However, the mechanisms by which the LTB₄–BLT1 axis relays chemotactic signals during intravascular neutrophil response to inflammation remain unclear. Here, we report that LTB₄ produced by neutrophils acts as an autocrine/paracrine signal to direct the vascular recruitment, arrest, and extravasation of neutrophils in a sterile inflammation model in the mouse footpad. Using intravital subcellular microscopy, we reveal that LTB₄ elicits sustained cell polarization and adhesion responses during neutrophil arrest *in vivo*. Specifically, LTB₄ signaling coordinates the dynamic redistribution of non-muscle myosin IIA and β₂-integrin, which facilitate neutrophil arrest and extravasation. Notably, we also found that neutrophils shed extracellular vesicles in the vascular lumen and that inhibition of extracellular vesicle release blocks LTB₄-mediated autocrine/paracrine signaling required for neutrophil arrest and extravasation. Overall, we uncover a novel complementary mechanism by which LTB₄ relays extravasation signals in neutrophils during early inflammation response.

Introduction

Neutrophils are the first mediators of innate immune responses (Lämmermann and Kastenmüller, 2019; Liew and Kubes, 2019). As they begin their journey to reach sites of inflammation, neutrophils in blood vessels respond by rolling on and adhering to the endothelium before extravasating to the interstitium (a process known as “transendothelial migration”; Lämmermann and Kastenmüller, 2019; Zarbock and Ley, 2008), where they further migrate directionally by sensing chemotactic gradients. Neutrophils respond to primary chemoattractants, such as formylated peptides and complement 5a (C5a), by producing the lipid mediator leukotriene B₄ (LTB₄) through the activity of the 5-lipoxygenase Alox5 (Majumdar et al., 2014; Werz, 2002). LTB₄ acts on its cognate receptor BLT1 to relay chemotactic signals to neighboring neutrophils, thereby broadening their recruitment range to the inflamed sites (Afonso et al., 2012; Lämmermann et al., 2013), where neutrophils engage with the microenvironment, secrete a variety of effector molecules, and help recruit other immune cells to promote host defense in a timely manner (Liew and Kubes, 2019).

Studies in mice that do not produce LTB₄ (Alox5^{−/−}) or lack its receptor (Bltl^{−/−}) have highlighted a critical role for the LTB₄–BLT1 axis in mobilizing neutrophils and other myeloid cells to sites of inflammation across multiple animal models (Collin et al., 2004; Tager et al., 2000). In fact, neutrophils self-orchestrate their recruitment during arthritis using a complex chemoattractant cascade that involves LTB₄ production in response to C5a, which proposedly functions in an autocrine manner to promote neutrophil extravasation (Miyabe et al., 2017; Sadik et al., 2012). LTB₄ production in neutrophils has also been shown to act in a paracrine fashion for the recruitment of both neutrophils and T cells in a chronic skin allergy model in mice (Oyoshi et al., 2012). However, the precise mechanism by which the autocrine/paracrine LTB₄–BLT1 axis functions to relay chemotactic signals leading to neutrophil extravasation has yet to be determined. To this end, we used an *in vivo* model system based on the use of intravital subcellular microscopy (ISMic), which allows the imaging of dynamic biological processes in live animals at subcellular resolution (Weigert et al., 2013; Ebrahim and Weigert, 2019). Here, we report a crucial role

¹Laboratory of Cellular and Molecular Biology, Center for Cancer Research, National Cancer Institute, National Institutes of Health, Bethesda, MD; ²Laboratory Animal Sciences Program, Leidos Biomedical Research, National Cancer Institute, National Institutes of Health, Bethesda, MD; ³Department of Pharmacology, University of Michigan, Ann Arbor, MI.

*R. Weigert and C.A. Parent are co-senior authors; Correspondence to Roberto Weigert: weigert@mail.nih.gov; Carole A. Parent: parentc@umich.edu.

This is a work of the U.S. Government and is not subject to copyright protection in the United States. Foreign copyrights may apply. This article is distributed under the terms of an Attribution–Noncommercial–Share Alike–No Mirror Sites license for the first six months after the publication date (see <http://www.rupress.org/terms/>). After six months it is available under a Creative Commons License (Attribution–Noncommercial–Share Alike 4.0 International license, as described at <https://creativecommons.org/licenses/by-nc-sa/4.0/>).

for neutrophil-derived LTB₄ in regulating the dynamics of the key regulators non-muscle myosin IIA (NMIIA) and β_2 -integrin (Itgb2), and that extracellular vesicles (EVs) from neutrophils mediate the autocrine/paracrine LTB₄/BLT1 signaling to promote neutrophil arrest and extravasation in live mice, thus complementing previously proposed mechanisms.

Results and discussion

The LTB₄–BLT1 axis is required for the persistent recruitment, arrest, and extravasation of neutrophils

To address the role of the LTB₄–BLT1 axis during neutrophil extravasation, we developed an *in vivo* inflammation model by injecting heat-killed *Escherichia coli* bioparticles (*E. coli* BPs) into the hind footpad of anesthetized mice (Fig. S1 A). First, we optimized conditions to image neutrophil extravasation behavior in a mouse strain that expresses GFP in myeloid cells (*LyzM-GFP*; Faust et al., 2000). Upon injection of *E. coli* BPs, neutrophils accumulated in the blood vessels and extravasated, whereas upon saline injection, they freely flowed in the vasculature (Fig. S1 A and Video 1). A similar effect was observed using an adoptive transfer model in which neutrophils purified from the bone marrow of a WT mouse were labeled with a cell-permeant fluorescent dye and transferred to a recipient WT mouse (Fig. 1 A and Video 2). To determine whether LTB₄ generated by neutrophils is required to drive their extravasation, we inflamed the footpads of *Alox5*^{−/−} mice, which are incapable of producing LTB₄, and introduced neutrophils purified from either WT or *Alox5*^{−/−} mice. We observed that up to 3.5 h postinjection, the recruitment of *Alox5*^{−/−} neutrophils to the infected footpad was significantly reduced compared with WT neutrophils (Fig. 1, B and C). To gain further insight into this process, we used the same model to visualize neutrophil intravascular dynamics (Video 3). Quantitative analysis revealed that ~60% of WT neutrophils displayed rolling, ~40% showed arrest in the lumen of the blood vessels, and ~20% extravasated in response to inflammation (Fig. 1, D–G). Conversely, *Alox5*^{−/−} neutrophils displayed significantly reduced arrest (<10%) and extravasation response (<5%), which correlated with an increased rolling response (>80%; Fig. 1, D–G). A similar defect was also observed in *Bltl*^{−/−} neutrophils, which lack the receptor for LTB₄ (Fig. 1, D–G). We complemented these results by investigating the intravascular dynamics of WT, *Alox5*^{−/−}, and *Bltl*^{−/−} neutrophils introduced into *Bltl*^{−/−} mice (Video 4 and Fig. 1, H–K). As expected, on the one hand, *Bltl*^{−/−} neutrophils exhibited enhanced rolling and a significant defect in arrest and extravasation (Fig. 1, H–K). On the other hand, *Alox5*^{−/−} neutrophils displayed rolling, arrest, and extravasation responses comparable to those of WT neutrophils, indicating that *Alox5*^{−/−} neutrophils likely use LTB₄ generated by resident cells, including neutrophils, to undergo extravasation in *Bltl*^{−/−} mice (Fig. 1, H–K). This observation also suggests that under physiological conditions, the tissue environment is capable of producing the LTB₄ required for neutrophil extravasation. Collectively, these findings establish that production and sensing of LTB₄ in neutrophils is critical for arrest and extravasation responses *in vivo*.

The LTB₄–BLT1 axis promotes polarized redistribution of NMIIA and Itgb2 during neutrophil arrest *in vivo*

The actin-based motor NMIIA is a downstream target of LTB₄ signaling in neutrophils stimulated with primary chemoattractants (Afonso et al., 2012; Subramanian et al., 2018). To determine how NMIIA activity contributes to neutrophil extravasation, we injected *Alox5*^{−/−} mice with WT neutrophils pretreated with either Y27632, which inhibits Rho-kinase (ROCK), a key enzyme that controls the activation and assembly of NMIIA filaments (Amano et al., 1996), or (S)-nitro-blebbistatin (nBleb), which inhibits myosin II contractile activity (Kovács et al., 2004; Lucas-Lopez et al., 2005). We observed that pretreatment with either Y27632 or nBleb, but not the vehicle, significantly reduced both arrest and extravasation in the first 45 min after neutrophil transfer (Fig. 2, A–C), consistent with a reported requirement of NMIIA for neutrophil extravasation *in vivo* (Zehrer et al., 2018). However, after 45 min, as the inhibitors were cleared, both neutrophil arrest and extravasation resumed similar to vehicle controls, indicating that the effects we observed were not due to drug toxicity (Fig. S1, B–D). These findings led us to address whether the LTB₄–BLT1 axis regulates NMIIA dynamics during neutrophil extravasation *in vivo*. To this end, neutrophils purified from a knock-in mouse expressing GFP-NMIIA (Milberg et al., 2017) were pretreated with either vehicle or MK886, a covalent nonreversible inhibitor of the 5-lipoxygenase adapter protein (Gillard et al., 1989). First, we determined that the extent of arrest and extravasation of the vehicle-treated GFP-NMIIA neutrophils was consistent with that of vehicle-treated WT neutrophils (Fig. 2, D–F vs. Fig. 2, A–C). Second, we found that treatment with MK886 led to reduced arrest and extravasation of GFP-NMIIA neutrophils (Fig. 2, D–F), consistent with our observations using *Alox5*^{−/−} neutrophils. Next, we used ISMic to visualize GFP-NMIIA dynamics in neutrophils that displayed arrest within the vasculature (Video 5) and to score for its cellular distribution during the arrest response. We found that although NMIIA redistributed from the cytoplasm to the cell cortex in the vehicle-treated neutrophils, this response was impaired upon MK886 treatment (Fig. 2, G and H; Fig. S1 E; and Video 5). This finding established that LTB₄ signaling in neutrophils is required for the persistent polarized redistribution of NMIIA *in vivo*. We also attempted to address the impact of the LTB₄–BLT1 axis on F-actin dynamics during extravasation using neutrophils derived from a mouse expressing the F-actin probe GFP-Lifeact (Riedl et al., 2010). Unfortunately, although GFP-Lifeact neutrophils exhibited rolling and arrest, they were defective in extravasation (not shown), suggesting a possible inhibitory effect of this probe. Overall, we conclude that the LTB₄–BLT1 axis promotes sustained cortical redistribution of NMIIA, which augments neutrophil arrest and extravasation *in vivo*.

Although NMIIA likely provides the contractile force required for neutrophils to squeeze through extravasation sites, its role during arrest is less clear. Therefore, we further investigated this aspect *in vivo*. Leukocyte arrest in the inflamed vessels, in most tissues, requires the engagement of Itgb2 on the plasma membrane (PM) with intercellular adhesion molecules presented on the inflamed endothelium (Liew and Kubes, 2019). Consistent with this notion, we found that *Itgb2*^{−/−} neutrophils,

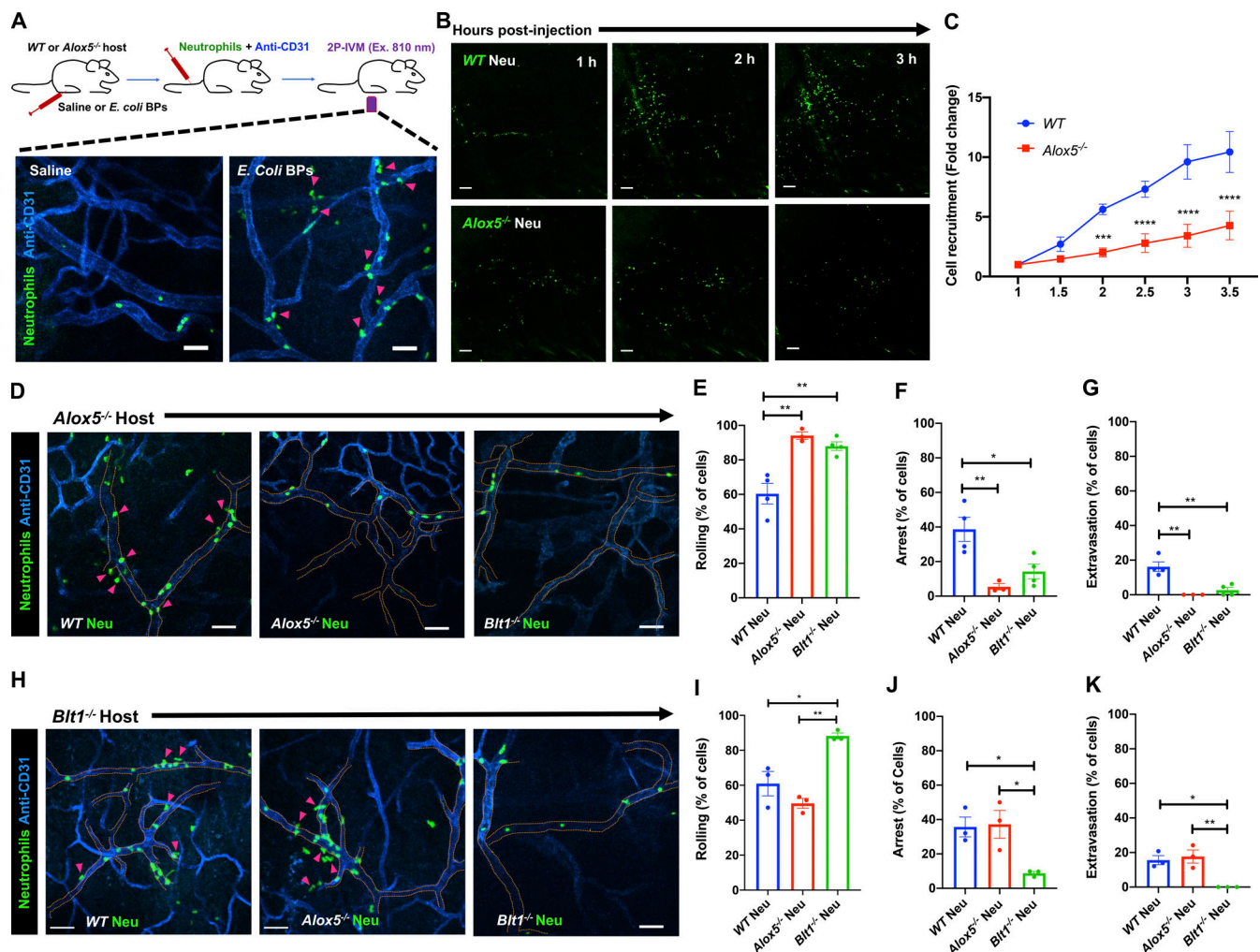


Figure 1. Production and sensing of LTB_4 via BLT1 in neutrophils promotes recruitment, arrest, and extravasation response in vivo. (A) Upper panel: Diagram of the 2P-IVM procedures in the footpad of an adoptive transfer mouse model. Lower panels: Neutrophils purified from WT mouse strains were labeled with CellTracker Green CMFDA and adoptively transferred to recipient WT mice that were injected in the footpad with either saline (left panel) or *E. coli* BPs (right panel) and imaged by 2P-IVM. Maximum projections of Z-stacks are shown (vasculature in blue and neutrophils in green). Pink arrowheads mark extravasating neutrophils (right panel). Scale bars = 50 μ m. The experiments were performed in $n = 2$ mice. See Video 2. (B and C) Neutrophils purified from either WT (upper panels) or *Alox5^{-/-}* (lower panels) mice were labeled with CellTracker Green CMFDA and adoptively transferred to *Alox5^{-/-}* mice with inflamed footpads. Maximum projections of Z-stacks of the footpads are presented for 1 h, 2 h, and 3 h after injection (B). Scale bars = 100 μ m. The number of neutrophils recruited to the footpad were scored and expressed as fold change with respect to the number of neutrophils at 1 h post-inflammation (C). Data are plotted as mean \pm SEM with $n = 3$ mice per condition. Two-way ANOVA using Sidak's multiple comparisons test was performed to determine statistical significance. (D–K) Neutrophils purified from WT or *Alox5^{-/-}* or *Blt1^{-/-}* mice were labeled with CellTracker Green CMFDA and adoptively transferred to *Alox5^{-/-}* (D–G) or *Blt1^{-/-}* (H–K) mice with inflamed footpads. 2P-IVM time-lapse images were acquired 1.5 h after *E. coli* BP injection (Videos 3 and 4). Still images represent maximum-intensity projections of Z-stacks in *Alox5^{-/-}* (D) or *Blt1^{-/-}* (H) mice. Dashed tangerine lines indicate vessel boundaries (blue), and magenta arrowheads point to extravasating neutrophils (green). Scale bars = 50 μ m. Neutrophils were scored for rolling (E and I), arrest (F and J), and extravasation (G and K) response in *Alox5^{-/-}* and *Blt1^{-/-}* mice, respectively, as described in the Materials and methods section. Data are plotted as the percentage of neutrophils exhibiting a specific behavior and represented as mean \pm SEM. Each dot represents the result from an individual animal. One-way ANOVA using Dunnett's multiple comparisons test was performed to determine statistical significance. *, $P < 0.05$; **, $P < 0.01$; ***, $P < 0.001$; ****, $P < 0.0001$.

when compared with WT neutrophils, displayed increased rolling as well as severe defects in arrest and extravasation when introduced in *Alox5^{-/-}* mice with inflamed footpads (Fig. 3, A and B), similar to our observations with *Alox5^{-/-}* neutrophils. Also, LTB_4 -stimulated neutrophils use Itgb2 on the PM to engage with the intercellular adhesion molecule-1-coated surface in vitro (Colom et al., 2015). We therefore hypothesized that the LTB_4 -BLT1-NMIIA pathway regulates the dynamics and localization of Itgb2 at the PM to promote firm neutrophil arrest. To directly

visualize Itgb2 dynamics, we incubated WT or *Alox5^{-/-}* neutrophils with a fluorescently conjugated antibody to Itgb2 (M18/2 clone) and introduced them into *Alox5^{-/-}* mice (Fig. 3 C). The antibody bound specifically to Itgb2 and did not qualitatively impact the extravasation response of labeled WT neutrophils in vivo (Fig. 3, C and D; and Video 6). In WT neutrophils that rolled along the blood vessel, Itgb2 localized in cytoplasmic clusters (Fig. 3 D, left panel; and Video 6). As the WT neutrophil underwent arrest, Itgb2 redistributed to areas of the cell periphery that

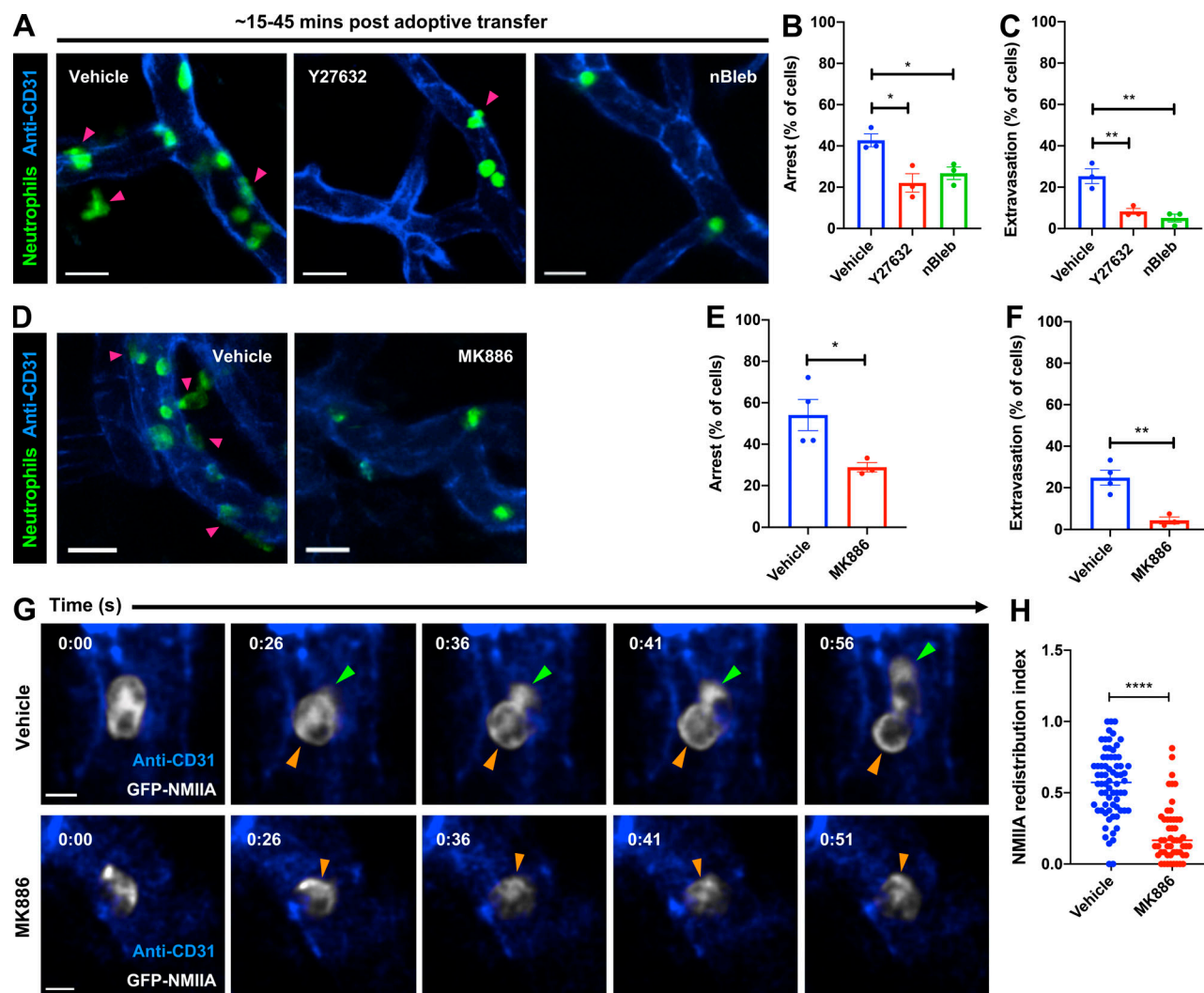


Figure 2. Cortical redistribution of NMIIA during neutrophil arrest requires the LTB_4 -BLT1 signaling axis. (A–C) Neutrophils purified from WT mice were stained with CellTracker Green CMFDA, treated with 40 μ M Y27632 or 10 μ M nBleb or vehicle (DMSO) for ~30 min, adoptively transferred into *Alox5*^{-/-} mice with inflamed footpads, and imaged by 2P-IVM. Maximum intensity projections of Z-stacks are presented (A). Magenta arrowheads highlight neutrophils (green) extravasating from the blood vessels (blue). Scale bars = 20 μ m. Quantification of the percentage of neutrophils that exhibited arrest (B) or extravasation (C) during the first 15–45 min after neutrophil transfer. Data are plotted as mean \pm SEM from $n = 3$ mice for each condition, and each dot represents the result from an individual animal. An unpaired *t* test with Welch's correction was used to determine statistical significance. (D–H) Neutrophils purified from *GFP-NMIIA* mice were treated with either 5 μ M MK886 or the vehicle (DMSO), adoptively transferred into *Alox5*^{-/-} mice with inflamed footpads, and imaged by ISMic. Maximum-intensity projections of Z-stacks are presented (D). Magenta arrowheads highlight extravasating *GFP-NMIIA* neutrophils (green) from the blood vessels (blue). Scale bars = 20 μ m. Quantification of the percentage of neutrophils that exhibited arrest (E) or extravasation (F) response. Data are plotted as mean \pm SEM; $n = 4$ mice for vehicle and $n = 3$ mice for the MK886 treatment; each dot represents the result from an individual animal. Unpaired *t* test with Welch's correction was used to determine statistical significance. Still images in G represent an individual optical slice from a Z-stack acquired in time-lapse mode (see Video 5). *GFP-NMIIA* is shown in white, and blood vessels are shown in blue. Green arrowhead points to the protrusive front of the extravasating neutrophil. Orange arrowheads indicate a region of cortical NMIIA enrichment. Time is represented in min:s. Scale bars = 5 μ m. The cortical redistribution of NMIIA was determined as described in the Materials and methods section and in Fig. S1 E and represented as redistribution index (H). Data points represent 70 cells from $n = 4$ mice for the vehicle and 51 cells from $n = 3$ mice for MK886 treatment, with each dot representing the value of a single cell. Unpaired *t* test with Welch's correction was used to determine statistical significance. *, $P < 0.05$; **, $P < 0.01$; ****, $P < 0.0001$.

were in direct contact with the endothelium (Fig. 3 D, middle panel; and Video 6). Later, as the WT neutrophil protruded and extravasated out of the vessel, Itgb2 gradually redistributed to the back of the migrating cell (Fig. 3 D, right panel; and Video 6), consistent with the previously observed high-affinity and clustering patterns of Itgb2 isoforms during neutrophil extravasation in vivo (Hyun et al., 2019). Conversely, Itgb2 remained dispersed in the cytoplasm and failed to redistribute to the cell periphery in

Alox5^{-/-} neutrophils that transiently underwent arrest response (Fig. 3, E and F; and Video 6). A similar defect in Itgb2 redistribution was also observed in WT neutrophils that were pretreated with either Y27632 or nBleb (Fig. 3 F), indicating a requirement for NMIIA in this process. These findings suggest that NMIIA activation downstream of LTB_4 signaling facilitates the dynamic redistribution and sustained localization of Itgb2 on the neutrophil PM to promote arrest response in the inflamed endothelium.

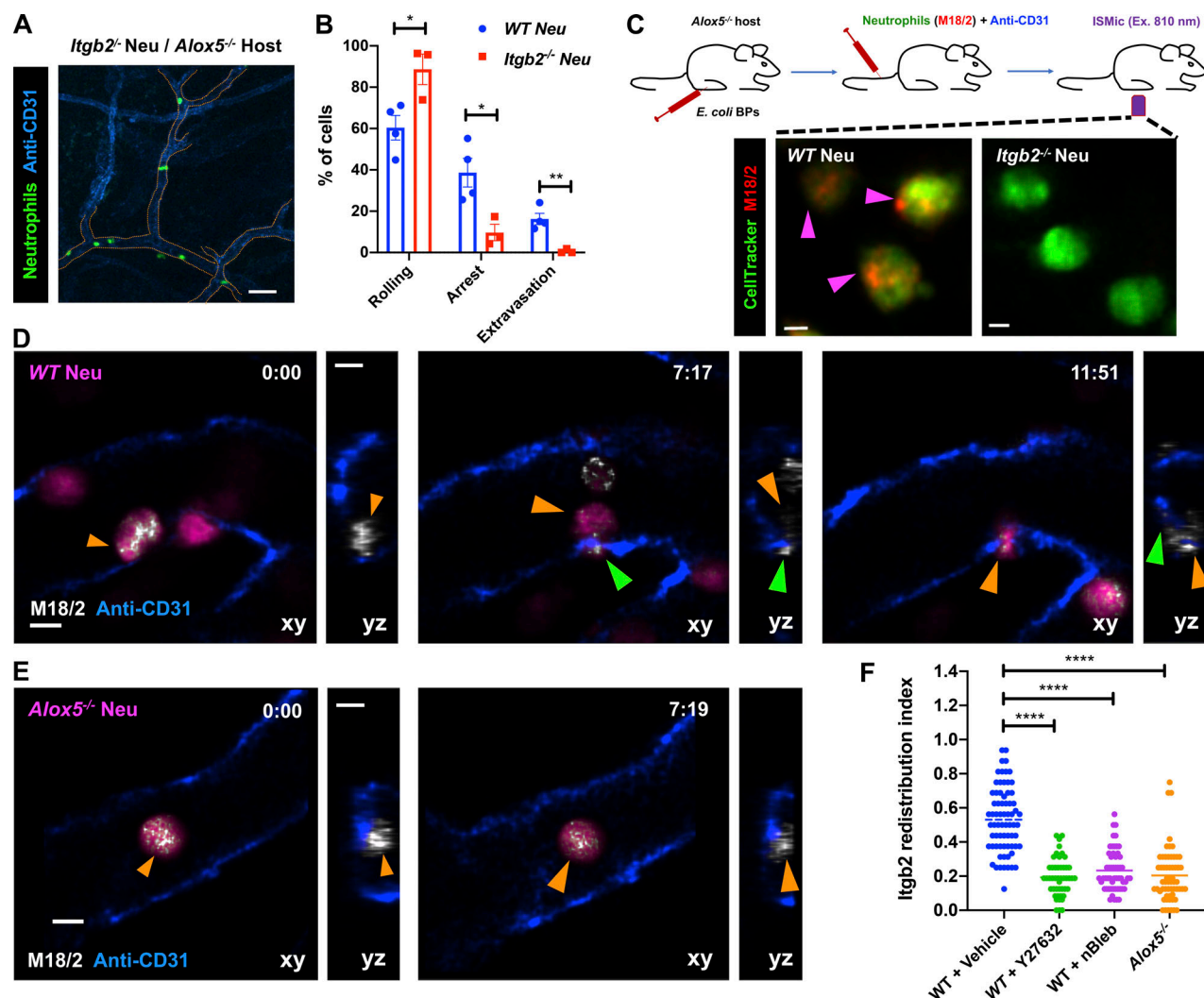


Figure 3. LTB₄-BLT1 axis regulates Itgb2 dynamics during neutrophil extravasation in vivo. (A and B) Neutrophils purified from *Itgb2^{-/-}* mice were labeled with CellTracker Green CMFDA, adoptively transferred into *Alox5^{-/-}* mice with inflamed footpads, and imaged by 2P-IVM. Maximum-intensity projection of a Z-stack (A). Dashed tangerine lines indicate vessel boundaries. Scale bar = 50 μ m. Quantitative analysis of the percentage of neutrophils that exhibit rolling, arrest, and extravasation response in *Itgb2^{-/-}* neutrophils compared with WT counterpart (B). Values for WT neutrophils are the same as in Fig. 1 E–G. Data are plotted as mean \pm SEM, and each dot represents the result from an individual animal. An unpaired *t* test with Welch's correction was used to determine statistical significance. (C) Neutrophils purified from either WT or *Itgb2^{-/-}* mice were labeled with CellTracker Green CMFDA and a fluorescently conjugated antibody against mouse Itgb2 (M18/2 clone, red), adoptively transferred into *Alox5^{-/-}* mice with inflamed footpads, and imaged by ISMic (top panel). Maximum-intensity projections of Z-stacks are presented (bottom panels). Magenta arrowheads indicate neutrophils positive for Itgb2 staining. The results represent *n* = 3 mice per condition. Scale bars = 3 μ m. (D–F) Neutrophils purified from either WT or *Alox5^{-/-}* mice were labeled with CellTracker Green CMPTX and fluorescently conjugated M18/2 antibody (red), adoptively transferred into *Alox5^{-/-}* mice with inflamed footpads, and imaged by ISMic. Additionally, WT neutrophils were pretreated with either vehicle (DMSO; D and F) or 40 μ M Y27632 (F) or 10 μ M nBleb (F) and transferred into the recipient. Still images represent maximum-intensity projections in x–y (large panels) and z–y (side panels) dimensions, derived from time-lapse sequences in Video 6 (min:s) for WT neutrophils (D) and *Alox5^{-/-}* neutrophils (E). CellTracker is shown in magenta, blood vessels in blue, and anti-Itgb2 in white. Orange and green arrowheads indicate the back and protrusive front of arrested and extravasating neutrophils, respectively. Scale bars = 5 μ m. The Itgb2 redistribution index was measured as described in the Materials and methods section and is presented as individual points for individual cells of WT (DMSO treated; 70 cells), WT + Y27632 (47 cells), WT + nBleb (54 cells), and *Alox5^{-/-}* (59 cells) from *n* = 3 mice per condition (F). One-way ANOVA using Dunnett's multiple comparisons test was performed to determine statistical significance. *, *P* < 0.05; **, *P* < 0.01; ****, *P* < 0.0001.

The LTB₄-BLT1 axis promotes adhesion, actomyosin polarization, and Itgb2 trafficking in primary neutrophils in vitro

LTB₄ has been shown to act as a signal relay molecule to promote chemotaxis of primary human neutrophils (polymorphonuclear neutrophils [PMNs]) in response to primary chemoattractant (Afonso et al., 2012). Because we found that the LTB₄-BLT1 axis

is required for neutrophil arrest in mice, we asked if such a mechanism operates during PMN adhesion in response to primary chemoattractant stimulation. To this end, we analyzed stimulation-induced adhesion of PMNs on a fibrinogen-coated surface. PMNs pretreated with vehicle showed a progressive increase in their ability to adhere upon stimulation with the bacterial peptide analogue fNLFNYK (Fig. 4 A). However,

pretreatment with MK886 or LY223982, a BLT1 antagonist (Jackson et al., 1992), significantly reduced PMN adhesion at later time points (Fig. 4 A). Importantly, the requirement of the LTB₄-BLT1 axis for sustained PMN adhesion was specific to end-target (fNLFNYK and C5a) but not intermediate (CXCL8) chemoattractants (Fig. S2 A), consistent with the notion that the LTB₄-BLT1 axis functions downstream of end-target or primary chemoattractants (Afonso et al., 2012; Sadik et al., 2012; Subramanian et al., 2018). Similarly, mouse neutrophils from *Bltl*^{-/-} mice adhered significantly less when compared with their WT counterparts upon stimulation with the bacterial peptide analogue WKYMVm (Fig. S2 B). Moreover, neutrophils from *GFP-NMIIA* mice adhered to an extent similar to that of WT control animals upon WKYMVm stimulation (Fig. S2 C). However, treatment with MK886 or LY223982, as compared with the vehicle control, significantly reduced the extent of adhesion of *GFP-NMIIA* neutrophils (Fig. S2 D), as we observed in PMNs. Importantly, MK886 or LY223982 treatment reduced the extent of cortical *GFP-NMIIA* and polarized F-actin distribution in *GFP-NMIIA* neutrophils in response to WKYMVm stimulation (Fig. S2, E and F). Similarly, a defect in cortical actomyosin distribution was also observed in PMNs upon treatment with MK886 or LY223982 (Fig. 4, B–D). Therefore, the LTB₄-BLT1 axis relays signals to promote sustained actomyosin polarity and adhesion of primary neutrophils downstream of primary chemoattractant stimulation.

Although we employed ISM_{ic} in the past to track endocytic events in other organ systems (Masedunskas and Weigert, 2008; Shitara et al., 2019), because of the depth of imaging in the mouse footpad, we could not image the trafficking of the Itgb2-containing intracellular structures with sufficient temporal and spatial resolution in vivo. Therefore, we used time-lapse confocal imaging to study the dynamics of human Itgb2 (ITGB2) in PMNs. To this end, we used an Alexa Fluor 488-conjugated antibody to label ITGB2 (CTB104 clone, hereafter called “fluorescent αITGB2”) in PMNs. We found that as PMNs began spreading upon fNLFNYK stimulation, ITGB2 quickly redistributed along the PM to form a ringlike structure at the interface of PMN contact with the fibrinogen-coated surface (Fig. 4 E, white arrows; and Video 7 A), reminiscent of our observations using ISM_{ic} (Fig. 3) and previous in vitro findings (Rochon et al., 2000; Shaw et al., 2004). With time, the ringlike structure disassembled, and ITGB2-containing vesicles internalized from the back of polarized and migrating PMNs (Fig. 4 E, blue arrowheads; and Video 7 A). However, upon blocking LTB₄ signaling using LY223982, we observed an increase of ITGB2-containing vesicles rather than the formation of the ringlike structure (Fig. 4 F, blue arrowheads; and Video 7 B). Consistently, a significant increase in the extent of internalized ITGB2-containing vesicles upon LY223982 treatment was also observed (Fig. S2, G–I). This finding prompted us to further investigate the regulation of ITGB2 trafficking by the LTB₄-BLT1 axis in PMNs. In polarized vehicle-treated PMNs, we found that clusters of ITGB2 largely localized at the PM around the adhesion site (Fig. 4 G, i), as revealed by the quenching of fluorescence of the αITGB2 antibody following incubation with a cell-impermeant antibody directed against the fluorophore (Fig. 4 G, ii). However, in MK886-treated PMNs, most of the

αITGB2 fluorescence showed a punctate intracellular distribution, which persisted even after treatment with the quenching antibody (Fig. 4 G, iii and iv). Using inhibitors of specific endocytic pathways, we confirmed that the internalization of αITGB2 indeed occurred via a clathrin-independent and dynamin-dependent endocytic pathway (Fig. S2, J and K), as previously described (Fabbri et al., 2005). Moreover, treatment with inhibitors of either the LTB₄-BLT1 axis or ROCK increased the pool of internalized ITGB2 with respect to control (Fig. 4 H). Finally, the extent of increase in the internalized ITGB2 corresponded to a block in the recycling of ITGB2 back to the PM, because only ~15% of the internalized ITGB2 was cleared upon inhibition of the LTB₄-BLT1-myosin pathway compared with 60% in the control (Fig. 4 I). Together, these findings in PMNs unravel a role for the LTB₄-BLT1-myosin axis in promoting recycling of ITGB2 from an intracellular pool as well as its retention on the PM (Fig. S2 L), which is consistent with our ISM_{ic} analysis in live mice.

Overall, we found that NMIIA regulates integrin-based adhesion stability during neutrophil arrest, possibly via different nonexclusive mechanisms, as previously reported (Vicente-Manzanares et al., 2009). We document that Itgb2 redistributes from a dispersed intracellular pool to a defined area of the neutrophil surface that is juxtaposed to the inflamed endothelium (adhesion ring), consistent with previous in vivo and in vitro studies (Hyun et al., 2019; Jones et al., 1988; Shaw et al., 2004). At this stage, we cannot resolve whether Itgb2 clusters observed at the adhesion ring-like structures are formed through lateral diffusion or rapid internalization and recycling back to the PM. We favor the latter explanation because inhibition of the LTB₄-BLT1 axis resulted in (1) a lack of the Itgb2 adhesion ringlike structure, (2) increased Itgb2 internalization, and (3) impaired Itgb2 recycling to the PM. Notably, these defects were phenocopied upon inhibition of NMIIA activation, thus strongly linking NMIIA activity with Itgb2 trafficking in neutrophils. Whether NMIIA activation directly promotes Itgb2 recycling or negatively regulates its internalization has yet to be determined. However, the regulation of Itgb2 by NMIIA in vivo is likely indirect because Itgb2 and NMIIA are localized to the front and rear of arrested neutrophils, respectively. Because NMIIA activity is proposed to regulate lipid microdomains on the neutrophil PM (Hind et al., 2016), it is conceivable that NMIIA, at the rear of the cells, creates domains that limit Itgb2 internalization and force the rapid recycling of internalized Itgb2 to the front of cells, thus confining Itgb2 localization to adhesion sites on the PM. However, in the absence of the LTB₄-BLT1 axis, NMIIA-controlled microdomains might be impaired, resulting in enhanced internalization and reduced oriented Itgb2 recycling, likely diverting its trafficking to a slow recycling pathway. The net result would be a reduction in Itgb2 levels on the PM, leading to an impairment in arrest and consequently in neutrophil extravasation.

The autocrine/paracrine action of LTB₄ requires EV release from neutrophils

Because LTB₄ produced by neutrophils drives their arrest and extravasation in vivo, we investigated whether this process

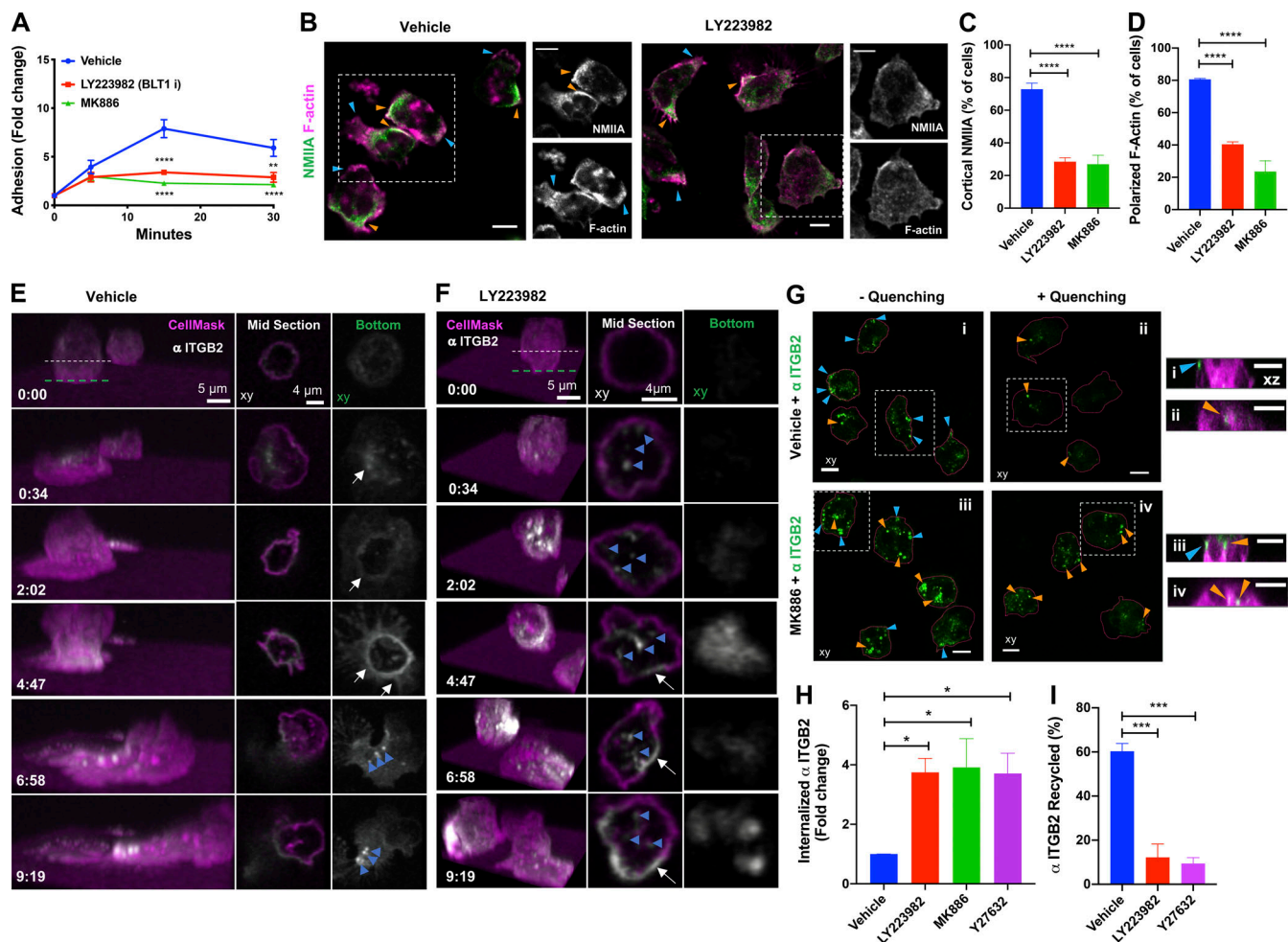


Figure 4. PMNs require LTB₄-BLT1 axis for sustained polarization, ITGB2 trafficking, and adhesion response in vitro. (A) PMNs were pretreated for 20 min with vehicle or 2 μ M MK886 or 20 μ M LY223982 and stimulated with 25 nM fNLNFK on a fibrinogen-coated surface. Cells remained either unstimulated (30 min) or were stimulated for 30, 15, and 5 min independently before fixation. Adhesion was calculated as described in the Materials and methods section and is presented as fold change of adhered neutrophils compared with unstimulated controls. Data are plotted as mean \pm SEM from $n = 3$ independent experiments. Two-way ANOVA using Dunnett's multiple comparisons test was performed to determine statistical significance. (B–D) PMNs were pretreated with vehicle or 2 μ M MK886 or 20 μ M LY223982 for 20 min, stimulated with 25 nM fNLNFK for 15 min, fixed, and stained with rhodamine phalloidin (magenta) and anti-NMIIA (green). Representative confocal images for vehicle and LY223982 treated PMNs (B). Blue and orange arrowheads indicate the front and back of PMNs with polarized actomyosin distribution, respectively. Dashed white box indicates the region zoomed and presented on the right side for each condition, with individual channels in grayscale. Scale bars = 5 μ m. Quantification of the percentage of neutrophils exhibiting cortical NMIIA (C) and polarized F-actin (D) in response to the above-mentioned treatments. Data are plotted as mean \pm SEM from $n = 3$ independent experiments. One-way ANOVA using Dunnett's multiple comparisons test was performed to determine statistical significance. (E and F) PMNs were pretreated with either vehicle (E) or 20 μ M LY223982 (F) for 20 min. They were incubated with an Alexa Fluor 488-conjugated antibody against human ITGB2 (α ITGB2, CTB104 clone; white) in combination with CellMask Deep Red (magenta) for \sim 1 min before stimulation with 100 nM fNLNFK for 10 min on a fibrinogen-coated surface and acquired in 3D using time-lapse confocal microscopy. See Video 7. Left panel represents the 3D view of the cell as a function of time (min:s). Middle and right panels represent the middle and bottom slices, respectively, as indicated by the dashed lines in the 3D view. White arrows indicate the formation of ITGB2 ringlike structure. Blue arrowheads indicate ITGB2 vesicles. Images are representative of three independent experiments (see Fig. S2, G–I). (G) PMNs were labeled with CellMask Deep Red to visualize the PM (magenta) and with α ITGB2 (green), pretreated with either the vehicle or 2 μ M MK886 for 20 min, and stimulated with 25 nM fNLNFK on a fibrinogen-coated surface. Neutrophils were fixed and either left untreated (– quenching; i and iii) or treated with an anti-Alexa Fluor 488 antibody (+ quenching; ii and iv). Images represent the maximum-intensity projections in x–y (large panels on the left) dimension for each condition. The cells in dashed white boxes are represented in the x–z dimension in small panels on the right. Blue and orange arrowheads indicate surface and internalized α ITGB2 signals, respectively. Scale bars = 5 μ m. Images are representative of $n = 3$ independent experiments. (H and I) Internalization and recycling of ITGB2. PMNs were treated with vehicle or 2 μ M MK886 or 20 μ M LY223982 or 20 μ M Y27632 for 20 min and stimulated with 25 nM fNLNFK for 10 min on a fibrinogen-coated surface in the presence of α ITGB2 (H). Samples were processed and imaged as described in the Materials and methods section to determine the percentage of the internalized ITGB2. Data are plotted as mean \pm SEM from $n = 4$ independent experiments. PMNs were treated with the vehicle or 2 μ M MK886 or 20 μ M LY223982 or 20 μ M Y27632 for 20 min and stimulated with 25 nM fNLNFK for 15 min on a fibrinogen-coated surface in the presence of α ITGB2 (I). Samples were washed and either fixed or stimulated for an additional 45 min in the presence of fNLNFK and inhibitors before fixation. Samples were processed and imaged as described in the Materials and methods section to determine the extent of recycling of internalized Itgb2. Data are plotted as mean \pm SEM from $n = 3$ independent experiments. One-way ANOVA using Dunnett's multiple comparisons test was performed to determine statistical significance. *, $P < 0.05$; **, $P < 0.01$; ***, $P < 0.001$; ****, $P < 0.0001$.

occurs in an autocrine/paracrine fashion. If this is the case, we reasoned that the defects in arrest and extravasation observed in *Alox5^{-/-}* neutrophils should be rescued upon coinjection with WT neutrophils, which are capable of producing LTB₄ (Fig. S3, A and B). Indeed, *Alox5^{-/-}* neutrophils displayed robust rolling, arrest, and extravasation in the presence of vehicle-treated WT neutrophils (Fig. 5 A, i; Fig. 5 B; and Video 8), but not with MK886-treated WT neutrophils (Fig. 5 A, ii; Fig. 5 B; and Video 8). We next investigated whether LTB₄ release and signal relay occurred via EVs, as reported during neutrophil chemotaxis in vitro (Majumdar et al., 2016). Using ISMic, we observed large Itgb2-containing neutrophil-derived EVs, which rolled along and occasionally tethered to the inflamed endothelial surface facing the vascular lumen in the vicinity of extravasating neutrophils (Fig. 5, C and D; and Video 9). Because of the limits in resolution of light microscopy, we could not determine whether these large vesicles were shed as individual membranous compartments or clusters of smaller vesicles. Therefore, we examined whether their biogenesis and release shared any common machinery with the generation of EVs, which in neutrophils are regulated by both the neutral sphingomyelinase (N-SMase) and the small GTPase Rab27a (Majumdar et al., 2016). We found that the number of neutrophil-derived EVs in the vasculature was dramatically reduced in WT neutrophils pretreated with either the N-SMase inhibitor GW4869 (Luberto et al., 2002) or the Rab27a inhibitor Nexinhib20 (Johnson et al., 2016; Fig. 5 E). However, blocking NMIIA contractility (nBleb) and lack of LTB₄ production (*Alox5^{-/-}*) or Itgb2 (*Itgb2^{-/-}*) did not impact the number of EVs observed in the vasculature (Fig. 5, E and F).

On the basis of these findings, we speculated that EVs could mediate the autocrine/paracrine actions of LTB₄ (Fig. S3 C). This hypothesis was confirmed by the fact that WT neutrophils pretreated with either GW4869 (Feng et al., 2003) or Nexinhib20, but not the control drug Exo1, failed to rescue the defect in arrest and extravasation of *Alox5^{-/-}* neutrophils (Fig. 5 A, i and iii–v; Fig. 5 B; and Video 8). We found that, consistent with these results, the inhibitors of EV release reduced actomyosin polarization, enhanced ITGB2 internalization, and impaired adhesion in PMNs stimulated with fNLFNYK in vitro (Fig. S3, D–G). Moreover, treatment with Nexinhib20 impaired the redistribution of Itgb2 in WT neutrophils in vivo (Fig. 5 G). Together, these findings suggest that neutrophil arrest and extravasation in vivo is mediated via EVs, which facilitate LTB₄ relay in an autocrine/paracrine manner (Fig. S4). This is, to our knowledge, the first evidence of an autocrine/paracrine LTB₄ signaling mechanism in vascular neutrophils that requires EVs, a mechanism in line with the emerging paradigm of the ability of EVs to relay chemotactic signals during amoeboid cell migration (Kriebel et al., 2018; Majumdar et al., 2016). Given the limitations of light microscopy, we document large neutrophil-derived EVs (size, ~1–2 μm) in the vasculature, similar to the EVs documented from neutrophils and tumor cells in vivo (Hoshino et al., 2015; Lai et al., 2015; Lim et al., 2015). The EVs we observed are similar to the microvesicles observed from the trailing edge of transmigrating neutrophils that get deposited in the perivascular area (Hyun et al., 2012). However, although the microparticles in transmigrating neutrophils have been

suggested to require Itgb2 (Hyun et al., 2012), the generation of EVs we observed did not require Itgb2 in neutrophils. Interestingly, the release of neutrophil-derived EVs in our model system requires N-SMase and Rab27 activity, which have previously been described to regulate the release of small EVs (Catalano and O'Driscoll, 2020; Majumdar et al., 2016; Raposo and Stoorvogel, 2013). However, whether such EVs harbor the LTB₄-synthesizing machinery and to what extent they use Itgb2 to tether to the inflamed endothelium remain to be ascertained.

In this study, we used two-photon intravital microscopy (2P-IVM) to investigate the specific mechanism by which the LTB₄-BLT1 axis signals during intravascular neutrophil response in the early phase of bacterial bioparticle-induced inflammation. Using pharmacological and genetic tools, we found that neutrophils undergo firm arrest and extravasation by producing and sensing LTB₄ in an autocrine/paracrine manner using an EV-based mechanism. Mechanistically, LTB₄ signaling is required for sustained actomyosin-based polarity, which ensures oriented vesicle trafficking and Itgb2 expression at the PM to promote persistent and productive interaction with the inflamed endothelium. Although neutrophils appear to be the major source of LTB₄ in our model system, it is conceivable that the LTB₄ produced from resident non-neutrophil cell types can contribute to the paracrine signaling under other physiological conditions.

An important aspect that we have not addressed in this study and that is currently under investigation is that of primary signals that initiate the LTB₄ cascade in neutrophils. Several mechanisms applicable to our model system could be occurring, such as exposure of tissue to (1) primary chemoattractants, which are sufficient to induce neutrophil extravasation from the exposed vessels (Hyun et al., 2019; Miyabe et al., 2017) through atypical receptors (Girbl et al., 2018; Miyabe et al., 2019); (2) bacteria, which stimulate perivascular macrophages to provide chemoattractant cues to direct neutrophil extravasation in dermal venules (Abtin et al., 2014); and (3) TNFα (Camussi et al., 1989) or bacterial lipopolysaccharide (Doerfler et al., 1989), which could prime neutrophils to generate LTB₄, possibly via ATP-gated calcium channels (Poplimont et al., 2020; Schumann et al., 1993). Once stimulated, autocrine/paracrine LTB₄/BLT1 signaling in neutrophils could likely function in conjunction with CXCL1 present on the inflamed endothelial surface to promote firm neutrophil arrest and potentiate neutrophil elastase secretion, which would help unseal endothelial junctions to facilitate CXCL2-guided neutrophil transmigration (Colom et al., 2015; Girbl et al., 2018).

We envision a scenario in which neutrophils, upon encountering primary signals, release EVs into the vasculature in proximity to the inflamed site. Given that EVs from stimulated neutrophils can use Itgb2 to anchor to the ECM and secrete neutrophil elastase to cleave the matrix (Genschmer et al., 2019), it is tantalizing to speculate that the EVs in the vasculature tether to the inflamed endothelium in an Itgb2-dependent fashion and locally release both LTB₄ and neutrophil elastase. LTB₄ and neutrophil elastase would in turn relay chemotactic signals to promote neutrophil arrest and to degrade endothelial junctions, respectively. Furthermore, as the inflammation

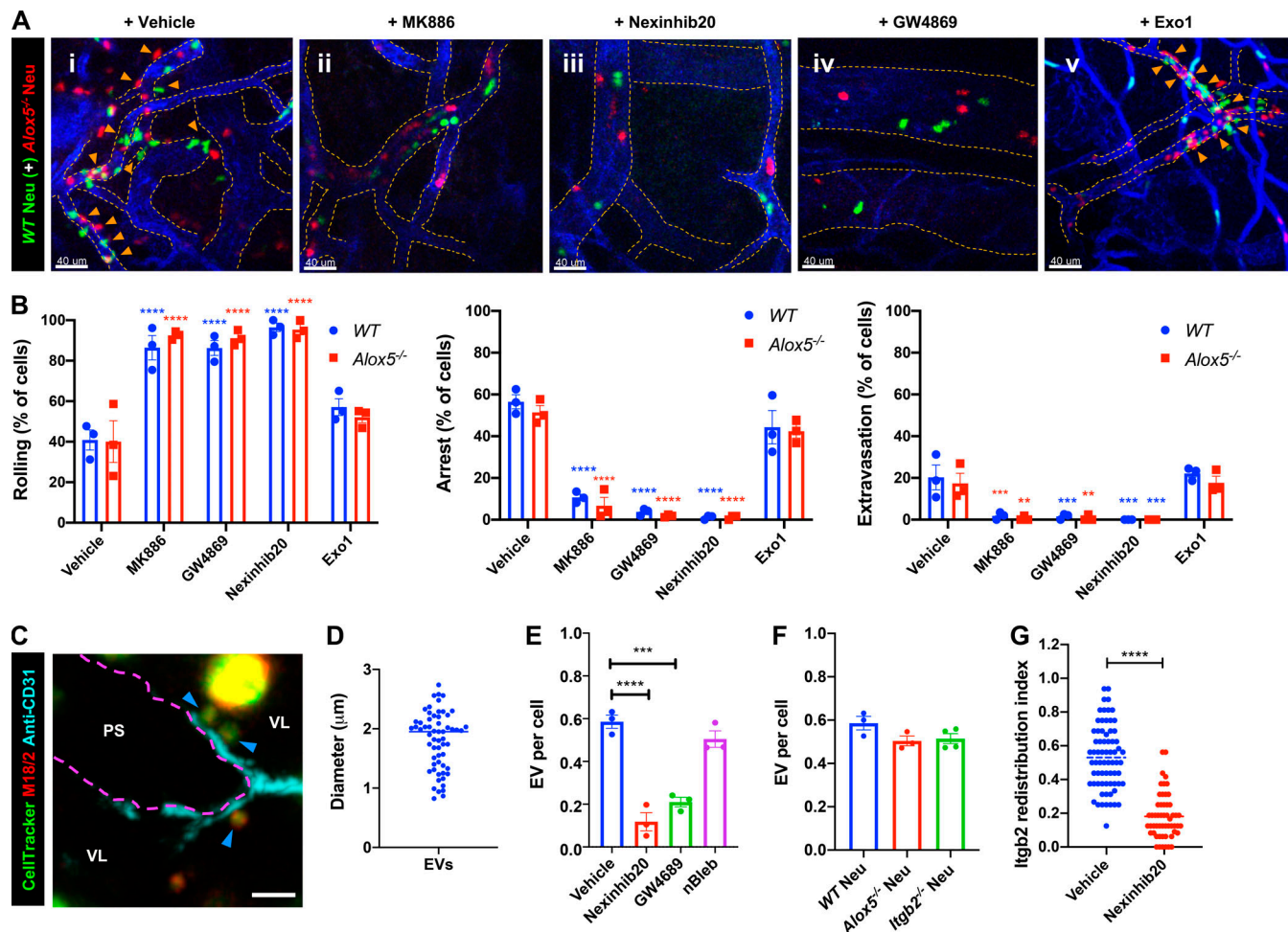


Figure 5. EVs mediate the autocrine/paracrine action of LTB_4 during neutrophil arrest and extravasation response. (A and B) WT neutrophils labeled with CellTracker Green CMFDA (green) were pretreated with vehicle (DMSO; i) or 5 μ M MK886 (ii), 2 μ M Nexinhib20 (iii), 20 μ M GW4689 (iv), or 40 μ M Exo1 (v) for 30 min and co-injected into $Alox5^{-/-}$ mice with inflamed footpads and $Alox5^{-/-}$ neutrophils labeled with CellTracker Red CMPTX (red). Maximum-intensity projections of Z-stacks acquired by 2P-IVM (A). See Video 8. Blood vessels are shown in blue, and dashed orange lines indicate vessel boundaries. Orange arrowheads point to extravasated neutrophils. Scale bars = 40 μ m. Analysis of the percentage of neutrophils displaying rolling, arrest, and extravasation in the above-mentioned conditions (B). Data are plotted as mean \pm SEM from $n = 3$ mice per group, and each dot represents the result from an individual animal. Two-way ANOVA using Dunnett's multiple comparisons test was performed to determine statistical significance. (C and D) WT neutrophils were labeled with CellTracker Green CMFDA (green) and fluorescently conjugated M18/2 antibody (red) before their adoptive transfer into $Alox5^{-/-}$ mice with inflamed footpads and imaged by ISMic. A representative maximum-intensity projection of a Z-stack with blood vessel in cyan (boundary marked with magenta dotted line); blue arrowheads indicate the EVs that rolled and tethered to the inflamed endothelial surface facing the vascular lumen (VL), and PS indicates the perivascular space (C). Scale bar = 5 μ m. See Video 9. Quantification of the size of EVs detected using ISMic analysis (D). Each dot represents the value of a single EV, and a total of 60 EVs were analyzed from $n = 3$ independent experiments. (E and F) Neutrophils purified from WT (E and F) or $Alox5^{-/-}$ (F) or $Itgb2^{-/-}$ (F) mice were labeled with CellTracker Green CMPTX and fluorescently conjugated M18/2 antibody (red), adoptively transferred into $Alox5^{-/-}$ mice with inflamed footpads, and imaged by ISMic. Additionally, WT neutrophils were pretreated with either vehicle (DMSO) or 2 μ M Nexinhib20 or 20 μ M GW4689 or 10 μ M nBleb for 30 min before their adoptive transfer into the recipient. The number of EVs detected was normalized to the number of detected neutrophils for each condition, as described in the Materials and methods section. Each dot represents the result from an individual animal experiment. Data are plotted as mean \pm SEM. One-way ANOVA using Dunnett's multiple comparisons test was performed to determine statistical significance, and no significant difference was observed in F. (G) Neutrophils purified from WT mice pretreated with either vehicle (DMSO) or 2 μ M Nexinhib20 for 30 min, labeled with CellTracker Green CMPTX and fluorescently conjugated M18/2 antibody (red), adoptively transferred into infected $Alox5^{-/-}$ mice with inflamed footpads, and imaged by ISMic. The peripheral Itgb2 redistribution index was determined as described in the Materials and methods section. Each dot represents the value for an individual cell, with values for WT vehicle control the same as in Fig. 3 F and $n = 54$ cells for Nexinhib20, from $n = 3$ mice for each group. An unpaired t test with Welch's correction was used to determine statistical significance. **, $P < 0.01$; ***, $P < 0.001$; ****, $P < 0.0001$.

proceeds, EVs could persistently engage with the inflamed vessels to serve as “beacons” to attract more neutrophils and other immune cells from the vasculature to follow the neutrophil path to inflamed sites (Lim et al., 2015; Oyoshi et al., 2012). Overall, our findings bear important clinical relevance

because LTB_4 production and EV generation in neutrophils are intimately associated with the progression of diseases, including tumor metastasis (Wculek and Malanchi, 2015) and chronic inflammatory lung disorder (Genschmer et al., 2019), respectively.

Materials and methods

Mice

The following strains were obtained from The Jackson Laboratory: C57BL/6J (WT), *Alox5^{-/-}* (B6.129S2-*Alox5^{tm1Fun}/J*), *Blt1^{-/-}* (B6.129S4-*Ltb4r1^{tm1Adl}/J*), and *Itgb2^{-/-}* (B6.129S7-*Itgb2^{tm1Bay}/J*). *LyzM-GFP*, *GFP-NMIIA*, and *GFP-Lifeact* mice were obtained from Drs. Dorian McGavern (National Institute of Neurological Disorders and Stroke, National Institutes of Health, Bethesda, MD), Robert Adelstein (National Heart, Lung, and Blood Institute, National Institutes of Health, Bethesda, MD), and Roland Wedlich-Söldner (Riedl et al., 2010), respectively. The study was approved and conducted in accordance with the animal protocols approved by the National Cancer Institute Institutional Animal Care and Use Committee (protocols LCMB-031 and LCMB-035). Mice, both males and females, were used for the experiments at an age between 2 and 6 mo.

Reagents

Antibodies against mouse *Itgb2* (clone M18/2; Alexa Fluor 594 conjugated), NMIIA heavy chain (clone Poly19098), and custom rhodamine-conjugated antibody to CD31 (clone 390) were obtained from BioLegend, Inc. Antibodies against CD31 (clone 390; eFluor 450 conjugated) and for quenching Alexa Fluor 488 (RRID AB_2532697) were purchased from Invitrogen. Antibodies against CD16/32 (Fc block; clone 2.4G2) and ITGB2 (clone CTB104; Alexa Fluor 488 conjugated) were obtained from BD PharMingen and Santa Cruz Biotechnology Inc., respectively. *E. coli* BPs (K12-strain; Texas red conjugated), CellTracker Green CMFDA, CellTracker Red CMTPX, CellMask Deep Red for PM, and rhodamine phalloidin dyes were obtained from Molecular Probes. PitStop2, monodansylcadaverine (MDC), fibrinogen (human plasma derived), and WKYMVM were purchased from MilliporeSigma. Recombinant fNLFNYK, human C5a, and human CXCL8 were obtained from Santa Cruz Biotechnology Inc., R&D Systems, and PeproTech Inc., respectively. LTB₄, LY223982, Y27632, nBleb, and GW4869 were purchased from Cayman Chemical. nBleb used in this study is a photostable version of blebbistatin (Lucas-Lopez et al., 2005). MK886, Nexinhib20, Exo1, dynasore, and MitMAB were obtained from Tocris Bioscience.

Primary neutrophil isolation from murine and human samples

Mouse neutrophils were obtained from the bone marrow of front and hind limbs. Briefly, cells were flushed out using RPMI without phenol red medium (Invitrogen) supplemented with 1 mM Gibco Hepes (Life Technologies) and antibiotics (Life Technologies; hereafter called "RPMI medium") and filtered via a 40-μm cell strainer (Corning Inc.). Subsequently, RBCs were lysed using ammonium-chloride-potassium (ACK) buffer (Life Technologies) for 30 s and then layered onto a discontinuous gradient of Histopaque 1077 (MilliporeSigma) and Histopaque 1119 (MilliporeSigma) in a 1:1:1 ratio as previously reported (Swamydas et al., 2015). Neutrophils were isolated from the 1077–1119 Histopaque interface, rinsed, and resuspended in RPMI medium. Human neutrophils (PMNs) were obtained from heparinized whole blood of healthy human donors by venipuncture as part of the National Institutes of Health Blood Bank

research program and purified from 1077 Histopaque–RPMI medium interface after differential centrifugation as reported previously (Subramanian et al., 2018). RBCs were then lysed by multiple rounds of exposure to hypotonic solution (0.2% NaCl solution; 30 s), followed by the addition of a neutralizing solution (1.6% NaCl solution) and then centrifugation. Isolated primary neutrophils were resuspended in RPMI medium and incubated on a rotator at RT for further experimentation. All the inhibitor treatments before chemoattractant stimulation in the *in vitro* experiments were performed at 37°C.

Adoptive transfer and inflammation model

Mouse neutrophils (~10⁷ cells) isolated from WT mice were labeled with cytosolic dye, either CellTracker Green CMFDA or CellTracker Red CMTPX, whereas neutrophils isolated from mice expressing GFP-NMIIA or GFP-Lifeact were used unstained. In select experiments, neutrophils were treated with inhibitors of LTB₄ production (MK886), ROCK activity (Y27632), NMIIA activity (nBleb), Rab27a (Nexinhib20), N-SMase (GW4869), ER-Golgi transfer (Exo1), or DMSO (0.2% in volume) as a vehicle control for 20–30 min at RT. For *Itgb2* visualization *in vivo*, DMSO- or inhibitor-treated neutrophils were incubated for 10 min with Fc-blocking antibody (2.5 μg per ~10⁷ cells), followed by 10-min incubation with anti-*Itgb2* antibody (M18/2 clone) conjugated to Alexa Fluor 594 (5 μg per ~10⁷ cells), washed, and adoptively transferred into the mice. Stained neutrophils (~6–8 × 10⁶) resuspended in saline were coinjected with antibody to CD31 (clone 390; 15 μg) conjugated to either rhodamine or eFluor 450 dye through tail vein injection. For co-adoptive transfer experiments, neutrophils purified (~6–8 × 10⁶ each) from WT mice and *Alox5^{-/-}* were labeled with different dyes, mixed in a 1:1 ratio, and adoptively transferred. The recipient mice were anesthetized by an intraperitoneal injection of a mixture of 100 mg/kg ketamine (VetOne) and 20 mg/kg xylazine (Anased LA; VetOne). Approximately 3–5 × 10³ *E. coli* BPs (~10–15 μl) were gently injected into the hind footpad using a syringe equipped with a 33-gauge needle (TSK Laboratory), without damaging the blood vessels and the tissue. In experiments involving inhibitors or ISMic, the recipient mice underwent short-term anesthesia by isoflurane inhalation (Forane; Baxter Healthcare Corp.), received an injection with *E. coli* BPs in the footpad, and were allowed to recover for 45 min before the adoptive transfer of neutrophils along with the conjugated anti-CD31 antibody. In the case of *LyzM-GFP* mice, the anti-CD31 antibody was injected *i.v.* before anesthesia. One footpad was injected with saline as a control, whereas the other was injected ~1 h afterward with *E. coli* BPs.

2P-IVM and ISMic of the infected footpad

The injected footpads of anesthetized mice were placed in a custom-designed holder to ensure stability, with the entire stage heated and maintained at 37°C throughout the imaging period. Imaging was performed by using an inverted laser-scanning two-photon microscope (MPE-RS; Olympus) equipped with a tunable laser (InSight DS+; Spectra Physics). Excitation was performed at 850 nm for the experiments with GFP-NMIIA neutrophils and at 810 nm for all the other experiments. Emitted

light was collected by an appropriate set of mirrors and filters on three GaAsP detectors (bandpass filters: blue = 410–460 nm; green = 495–540 nm; red = 575–645 nm). Images were acquired using a 37°C heated objective/10× air objective (NA 0.4) with 30× and 40× silicone oil immersion UPLSAPO objectives (NA 1.05 and 1.25, respectively; Olympus). Imaging was performed by continuous acquisition of 20–25 Z-stacks (3-μm step size and at a frame rate of ~6–10 s between frames) for a total period of 15–20 min for individual field of view (FOV). For ISMic, we used both 30× and 40× objectives, with a digital zoom of 2–4×, acquiring 8–10 Z-stacks with 2-μm step size and at a frame rate of ~6–10 s between frames for a total period of 5–10 min for individual FOV. Images were acquired using the Olympus Fluo-View software and processed for further analysis using Fiji, Imaris (Bitplane), and MATLAB (MathWorks). For representation in Videos 5 and 6, Fig. 2 D, and Fig. 3, D and E, ISMic images were further 3D deconvolved using AutoQuant X3 (Media Cybernetics) involving a blind adaptive method with theoretical point spread function and five iterations.

Analysis of neutrophil recruitment kinetics in the infected footpad

The maximal projection of Z-stacks shown in Fig. 1 B was acquired by 2P-IVM using a 10× air objective at fixed time points after inflammation. Maximal projections were used to quantify the neutrophils in each FOV using the Imaris spot detection function at each time point. A single FOV using the 10× air objective was sufficient to capture a large area with neutrophil recruitment response, which was followed over multiple time points. The numbers of neutrophils were normalized and represented as fold change with respect to 1 h after inflammation. The number of neutrophils observed at 1 h after inflammation observed in the footpad between adoptively transferred WT or *Alox5^{-/-}* neutrophils was comparable across experiments.

Analysis of intravascular neutrophil behavior

First, we corrected for the motion artifacts due to heartbeat and respiration by applying to the raw time-lapse images a customized MATLAB function based on a maximum cross-correlation image registration algorithm (Brown, 1992). Next, we determined the outline of the blood vessels for each time frame by segmentation of the maximal projections derived from the volume rendering of the acquired Z-stacks. Neutrophil contours were identified using a snake algorithm implemented with MATLAB scripts, as previously described (Chen et al., 2016; Xu and Prince, 1998), and they were overlaid to the maximum-intensity projection of the blood vessels. To measure neutrophil velocity, we used a manual tracking plugin in Fiji. To determine their position with respect to the blood vessels, we calculated the overlap fraction (OF). For each cell at each frame, the OF was calculated as the area of the 2D maximum projection of the cell overlapping with the segmented blood vessels divided by the total cell area. Neutrophils were considered inside the blood vessels if the OF exceeded 0.5. Neutrophils were classified as showing free-flowing, rolling, arrest, or extravasation behavior according to the following criteria: (1) free flowing if the velocity was >40 μm/s and the OF was >0.5, (2) rolling if the velocity was

between 2 and 40 μm/s (Sundd et al., 2011) and the OF was >0.5, (3) arrest if the velocity was <0.15 μm/s and remained at the same place for 30 s (Miyabe et al., 2017) or more with the OF >0.5, and (4) extravasation if the OF dropped below 0.5. The neutrophil behaviors were scored and were represented independently for each cell in the FOV. Because a neutrophil can show one or more behaviors during the course of acquisition, each behavior was independently scored, and therefore the percentage of cells that display rolling, arrest, and extravasation will not add up to 100% by this analysis. Multiple FOVs were imaged in each experiment, and typically datasets between 1–2 h after inflammation were considered for analysis, with the data normalized and presented as the percentage of cells across FOVs analyzed for rolling, arrest, and extravasation behavior for each experiment in each condition. For the experiments involving Y27632, nBleb, and MK886 treatments, the percentage of cells that arrested and extravasated were scored manually from multiple FOVs in each ISMic imaging experiment.

Analysis of peripheral distribution index and EVs

We acquired Z-stacks (typically 8–12 stacks) at a frame rate of ~5–8 s. Only neutrophils that displayed arrest behavior were considered for the time periods 0, 30, 60, and 90 s of arrest within the blood vessel. In every frame, we identified the sections corresponding to a given cell and determined the cortical redistribution of either GFP-NMIIA or Itgb2 by assigning a value of 0 for a centrally distributed fluorescent signal within the cell and a value of 1 for a cortically distributed fluorescent signal at the cell periphery. For each cell, we averaged the scores determined in each section of the stack to the total number of stacks analyzed across the time period, and the index for each cell analyzed was determined. The diameters of EVs were measured using Imaris software. The number of EVs detected across multiple FOVs was normalized to the number of detected neutrophils in the same for individual experiments per condition.

In vitro adhesion assay and the analysis of actomyosin polarity

Neutrophils (2×10^5 cells) were plated in eight-well chambers with a bottom cover glass coated with 100 μg/ml of fibrinogen (Lab-Tek; 1 NA). All the experiments were performed in RPMI medium at 37°C. Cells were pretreated with vehicle (DMSO; 0.2% in volume) or specified inhibitors for 20 min before stimulation with chemoattractants. After stimulation, cells were gently washed with RPMI medium, fixed with 4% PFA, and stained with DAPI (10 ng/ml) and rhodamine phalloidin (0.2 units). For the analysis of cortical distribution of NMIIA, cells were permeabilized with a buffer (0.5% saponin and 0.5% Triton X-100, both from MilliporeSigma) for 5 min at 37°C, followed by staining with anti-NMIIA antibody (in 1% FBS containing PBS) overnight at 4°C and thereafter with a secondary antibody for 2 h at RT. Images were acquired by using an 880 Airyscan microscope equipped with GaAsP detectors and using either a 20× (Zeiss Plan Apochromat 20×/NA 0.8, air) or 40× (Zeiss Plan Apochromat 40×/NA 1.4, oil) lens together with ZEN software (Carl Zeiss). The number of cells per FOV was estimated by measuring the DAPI signal using the Imaris spot detection method. Typically, >100 cells per condition were analyzed from

multiple FOVs. For the kinetic analysis of adhesion response reported in Fig. 4 A, the number cells from FOVs was averaged for each time point and represented as fold change with respect to unstimulated control. For the other experiments, results were normalized and represented as the percentage of the vehicle-treated controls. Rhodamine phalloidin and NMIIA staining was used to manually quantify the percentage of cells in each FOV exhibiting polarized F-actin and cortical NMIIA distribution and averaged for each condition in an experiment. Typically, ~100 cells or more per condition were analyzed from multiple FOVs in each experiment to determine actomyosin polarity in PMNs. For experiments involving GFP-NMIIA neutrophils, cells were fixed as above but only stained with DAPI and rhodamine phalloidin and analyzed as mentioned above.

Analysis of ITGB2 vesicle trafficking in vitro

For live-cell imaging, Alexa Fluor 488-conjugated anti-ITGB2 antibody (α ITGB2, CTB104 clone, 2 μ g) and CellMask Deep Red (100 nM) were added to vehicle- or inhibitor-treated PMNs suspended in RPMI medium and plated on fibrinogen-coated surface before stimulation with 100 nM fNLFNYK and thereafter imaging for ~10 min post-stimulation within an incubation chamber set at 37°C. Images were acquired in time-lapse mode by using an 880 Airyscan microscope using the 63 \times (Zeiss Plan Apochromat 63 \times /NA 1.4, oil) heated lens (37°C). For the analysis of ITGB2 internalization, Alexa Fluor 488-conjugated α ITGB2 (0.1 μ g/ml) was added to vehicle- or inhibitor-pretreated PMNs suspended in RPMI medium before stimulation with fNLFNYK at 37°C. After 10 min of stimulation, cells were fixed and incubated overnight at 4°C with an anti-Alexa Fluor 488 functional antibody (0.5 μ g per well) to quench the α ITGB2 signals on the PM. Samples were counterstained with DAPI and phalloidin. Internalized ITGB2 was detected using either epifluorescence (Revolve FL, FJSD1000; ECHO Laboratory) or confocal (Carl Zeiss 880 Airyscan microscope) microscopes equipped with 40 \times or 63 \times objectives. The Revolve FL epifluorescence microscope was equipped with a complementary metal oxide semiconductor camera and 40 \times (LUCPlan FL N) Olympus objective lens. The number of internalized fluorescent vesicles were determined using the Imaris spot detection method. Typically, >100 cells per condition were analyzed from multiple FOVs. Results were normalized and represented as the percentage or fold change with respect to the fluorescent vesicles detected in the control or vehicle condition. For the ITGB2 recycling experiments, vehicle- or inhibitor-treated PMNs were stimulated in the presence of Alexa Fluor 488-conjugated anti-ITGB2 antibody for 15 min. Cells were gently washed with RPMI and either fixed or incubated for an additional 45 min in RPMI containing fNLFNYK (with or without inhibitor) and anti-Alexa Fluor 488 functional antibody to allow recycling of internalized ITGB2. Cells were then fixed, and the α ITGB2 signals on the PM were further quenched as described above. The number of internalized fluorescent vesicles was determined using the Imaris spot detection method as described above. Results are presented as the percentage difference in the detected fluorescent vesicles relative to that of the 15-min time point.

Quantification and statistical analysis and representation

Microsoft Excel software was used for calculations, and the results were plotted and analyzed using Prism software (GraphPad Software, Inc.). Statistical tests for each graph and the size of the samples are described in the respective figure legends. For clarity, results from the 2P-IVM experiments are presented as scatterplots with bar graphs, and in vitro neutrophil stimulation experiments are presented as bar graphs.

Online supplemental material

Figs. S1, S2, and S3 support Figs. 1 and 2, 4, and 5, respectively. Fig. S1 describes the mouse footpad inflammation model. Fig. S2 summarizes results from primary human and mouse neutrophils. Fig. S2 K summarizes our observations on ITGB2 dynamics in PMNs. Fig. S3 shows the 2P-IVM procedure in *Alox5*^{-/-} mice used to study LTB₄ paracrine signaling in neutrophils. Fig. S4 presents a model based on our conclusions. Supplementary videos were generated using Adobe Photoshop software to assemble individual videos into one and for labeling/annotation purposes. Video 1 shows 2P-IVM of an *LyzM*-GFP mouse footpad at ~1 h after injection of saline into one footpad and *E. coli* BPs into the other. Video 2 shows 2P-IVM of the footpad in a WT mouse that received labeled WT neutrophils at ~1.5 h after injection of saline into one footpad and *E. coli* BPs into the other. Video 3 shows 2P-IVM of the inflamed *Alox5*^{-/-} mouse footpad at ~1.5 h, where labeled neutrophils were introduced from WT or *Alox5*^{-/-} or *Bltl*^{-/-} mice. Video 4 shows 2P-IVM of the inflamed *Bltl*^{-/-} mouse footpad at ~1.5 h, where labeled neutrophils were introduced from WT or *Alox5*^{-/-} or *Bltl*^{-/-} mice. Video 5 shows ISMic imaging of the inflamed footpad of an *Alox5*^{-/-} mouse that received either vehicle- or MK886-treated GFP-NMIIA neutrophils at ~1 h after inflammation. Video 6 shows ISMic imaging of the inflamed footpad of an *Alox5*^{-/-} mouse that received WT or *Alox5*^{-/-} neutrophils labeled for cytoplasm and *Itgb2* at ~1 h after inflammation. Video 7 shows confocal imaging of PMNs stained for PM and α ITGB2 that were pretreated with vehicle (DMSO) or BLT1 inhibitor (LY223982) for 20 min before stimulation with fNLFNYK and simultaneous live acquisition for 10 min. Video 8 shows 2P-IVM of the inflamed footpad at ~2 h, where labeled WT neutrophils that were pretreated with vehicle (DMSO) or the inhibitors MK886 or GW4689 or Nexinhib20 or Exo1 were co-injected with labeled *Alox5*^{-/-} neutrophils into *Alox5*^{-/-} mice. Video 9 shows ISMic imaging of WT neutrophils introduced into an *Alox5*^{-/-} mouse with an inflamed footpad at ~2 h, with EVs containing CellTracker Green CMFDA and *Itgb2*.

Acknowledgments

We thank Drs. Dorian McGavern (National Institute of Neurological Disorders and Stroke, Bethesda, MD) and Robert S. Adelstein (National Heart, Lung, and Blood Institute, Bethesda, MD) for providing the *LyzM*-GFP and GFP-NMIIA mouse lines, respectively. We thank the animal facilities of the National Cancer Institute and Dr. Wang-Ting Hsieh (Frederick National Laboratory for Cancer Research, Frederick, MD) for maintaining and genotyping the animals, respectively. We also thank Dr. Michael Kruhlak, Langston Lim, and Dr. Andy Tran at the

National Cancer Institute Center for Cancer Research confocal core for their help with confocal microscopy.

This research was supported by the intramural research program of the National Institutes of Health (ZIA BC 011682), the National Cancer Institute, and the National Cancer Institute Center for Cancer Research.

The authors declare no competing financial interests.

Author contributions: Conceptualization: B.C. Subramanian, R. Weigert, and C.A. Parent; Methodology: B.C. Subramanian, N. Melis, W. Wang, D. Gallardo, R. Weigert, and C.A. Parent; Investigation: B.C. Subramanian, N. Melis, and D. Gallardo; Analysis: B.C. Subramanian, D. Chen, and R. Weigert; Writing, original draft: B.C. Subramanian, R. Weigert, and C.A. Parent.

Submitted: 1 November 2019

Revised: 17 June 2020

Accepted: 23 July 2020

References

- Abtin, A., R. Jain, A.J. Mitchell, B. Roediger, A.J. Brzoska, S. Tikoo, Q. Cheng, L.G. Ng, L.L. Cavanagh, U.H. von Andrian, et al. 2014. Perivascular macrophages mediate neutrophil recruitment during bacterial skin infection. *Nat. Immunol.* 15:45–53. <https://doi.org/10.1038/ni.2769>
- Afonso, P.V., M. Janka-Junttila, Y.J. Lee, C.P. McCann, C.M. Oliver, K.A. Aamer, W. Losert, M.T. Cicerone, and C.A. Parent. 2012. LTB₄ is a signal-relay molecule during neutrophil chemotaxis. *Dev. Cell.* 22: 1079–1091. <https://doi.org/10.1016/j.devcel.2012.02.003>
- Amano, M., M. Ito, K. Kimura, Y. Fukata, K. Chihara, T. Nakano, Y. Matsuura, and K. Kaibuchi. 1996. Phosphorylation and activation of myosin by Rho-associated kinase (Rho-kinase). *J. Biol. Chem.* 271:20246–20249. <https://doi.org/10.1074/jbc.271.34.20246>
- Brown, L.G.. 1992. A survey of image registration techniques. *ACM Comput. Surv.* 24:325–376. <https://doi.org/10.1145/146370.146374>
- Camussi, G., C. Tetta, F. Bussolino, and C. Baglioni. 1989. Tumor necrosis factor stimulates human neutrophils to release leukotriene B₄ and platelet-activating factor: induction of phospholipase A₂ and acetyl-CoA:1-alkyl-sn-glycero-3-phosphocholine O₂-acetyltransferase activity and inhibition by antiproteinase. *Eur. J. Biochem.* 182:661–666. <https://doi.org/10.1111/j.1432-1033.1989.tb14876.x>
- Catalano, M., and L. O'Driscoll. 2020. Inhibiting extracellular vesicles formation and release: a review of EV inhibitors. *J. Extracell. Vesicles.* 9. 1703244. <https://doi.org/10.1080/20013078.2019.1703244>
- Chen, D., S. Sarkar, J. Candia, S.J. Florczyk, S. Bodhak, M.K. Driscoll, C.G. Simon, Jr., J.P. Dunkers, and W. Losert. 2016. Machine learning based methodology to identify cell shape phenotypes associated with micro-environmental cues. *Biomaterials.* 104:104–118. <https://doi.org/10.1016/j.biomaterials.2016.06.040>
- Collin, M., A. Rossi, S. Cuzzocrea, N.S.A. Patel, R. Di Paola, J. Hadley, M. Collino, L. Sautebin, and C. Thiemermann. 2004. Reduction of the multiple organ injury and dysfunction caused by endotoxemia in 5-lipoxygenase knockout mice and by the 5-lipoxygenase inhibitor zileuton. *J. Leukoc. Biol.* 76:961–970. <https://doi.org/10.1189/jlb.0604338>
- Colom, B., J.V. Bodkin, M. Beyrau, A. Woodfin, C. Ody, C. Rourke, T. Chavakis, K. Brohi, B.A. Imhof, and S. Nourshargh. 2015. Leukotriene B₄-neutrophil elastase axis drives neutrophil reverse transendothelial cell migration in vivo. *Immunity.* 42:1075–1086. <https://doi.org/10.1016/j.immuni.2015.05.010>
- Doerfler, M.E., R.L. Danner, J.H. Shelhamer, and J.E. Parrillo. 1989. Bacterial lipopolysaccharides prime human neutrophils for enhanced production of leukotriene B₄. *J. Clin. Invest.* 83:970–977. <https://doi.org/10.1172/JCI13983>
- Ebrahim, S., and R. Weigert. 2019. Intravital microscopy in mammalian multicellular organisms. *Curr. Opin. Cell Biol.* 59:97–103. <https://doi.org/10.1016/j.cob.2019.03.015>
- Fabbri, M., S. Di Meglio, M.C. Gagliani, E. Consonni, R. Molteni, J.R. Bender, C. Tacchetti, and R. Pardi. 2005. Dynamic partitioning into lipid rafts controls the endo-exocytic cycle of the $\alpha L/\beta_2$ integrin, LFA-1, during leukocyte chemotaxis. *Mol. Biol. Cell.* 16:5793–5803. <https://doi.org/10.1091/mbc.e05-05-0413>
- Faust, N., F. Varas, L.M. Kelly, S. Heck, and T. Graf. 2000. Insertion of enhanced green fluorescent protein into the lysozyme gene creates mice with green fluorescent granulocytes and macrophages. *Blood.* 96: 719–726. <https://doi.org/10.1182/blood.V96.2.719>
- Feng, Y., S. Yu, T.K.R. Lasell, A.P. Jadhav, E. Macia, P. Chardin, P. Melancon, M. Roth, T. Mitchison, and T. Kirchhausen. 2003. Exol: a new chemical inhibitor of the exocytic pathway. *Proc. Natl. Acad. Sci. USA.* 100: 6469–6474. <https://doi.org/10.1073/pnas.0631766100>
- Genschmer, K.R., D.W. Russell, C. Lal, T. Szul, P.E. Bratcher, B.D. Noerager, M. Abdul Roda, X. Xu, G. Rezonzew, L. Viera, et al. 2019. Activated PMN exosomes: pathogenic entities causing matrix destruction and disease in the lung. *Cell.* 176:113–126.e15. <https://doi.org/10.1016/j.cell.2018.12.002>
- Gillard, J., A.W. Ford-Hutchinson, C. Chan, S. Charleson, D. Denis, A. Foster, R. Fortin, S. Leger, C.S. McFarlane, H. Morton, et al. 1989. L-663,536 (MK-886) (3-[1-(4-chlorobenzyl)-3-t-butyl-thio-5-isopropylindol-2-yl]-2,2 - dimethylpropanoic acid), a novel, orally active leukotriene biosynthesis inhibitor. *Can. J. Physiol. Pharmacol.* 67:456–464. <https://doi.org/10.1139/y89-073>
- Girbl, T., T. Lenn, L. Perez, L. Rolas, A. Barkaway, A. Thiriot, C. Del Fresno, E. Lynam, E. Hub, M. Thelen, et al. 2018. Distinct Compartmentalization of the chemokines CXCL1 and CXCL2 and the atypical receptor ACKR1 determine discrete stages of neutrophil diapedesis. *Immunity.* 49: 1062–1076.e6. <https://doi.org/10.1016/j.immuni.2018.09.018>
- Hind, L.E., W.J.B. Vincent, and A. Huttenlocher. 2016. Leading from the back: the role of the uropod in neutrophil polarization and migration. *Dev. Cell.* 38:161–169. <https://doi.org/10.1016/j.devcel.2016.06.031>
- Hoshino, A., B. Costa-Silva, T.-L. Shen, G. Rodrigues, A. Hashimoto, M. Tesic Mark, H. Molina, S. Kohsaka, A. Di Giannatale, S. Ceder, et al. 2015. Tumour exosome integrins determine organotropic metastasis. *Nature.* 527:329–335. <https://doi.org/10.1038/nature15756>
- Hyun, Y.-M., R. Sumagin, P.P. Sarangi, E. Lomakina, M.G. Overstreet, C.M. Baker, D.J. Fowell, R.E. Waugh, I.H. Sarelius, and M. Kim. 2012. Uropod elongation is a common final step in leukocyte extravasation through inflamed vessels. *J. Exp. Med.* 209:1349–1362. <https://doi.org/10.1084/jem.20111426>
- Hyun, Y.-M., Y.H. Choe, S.A. Park, and M. Kim. 2019. LFA-1 (CD11a/CD18) and Mac-1 (CD11b/CD18) distinctly regulate neutrophil extravasation through hotspots I and II. *Exp. Mol. Med.* 51:1–13. <https://doi.org/10.1038/s12276-019-0227-1>
- Jackson, W.T., R.J. Boyd, L.L. Froelich, B.E. Mallett, and D.M. Gapinski. 1992. Specific inhibition of leukotriene B₄-induced neutrophil activation by LY223982. *J. Pharmacol. Exp. Ther.* 263:1009–1014.
- Johnson, J.L., M. Ramadass, J. He, S.J. Brown, J. Zhang, L. Abgaryan, N. Biris, E. Gavathiotis, H. Rosen, and S.D. Catz. 2016. Identification of neutrophil exocytosis inhibitors (Nexinhits), small molecule inhibitors of neutrophil exocytosis and inflammation: druggability of the small GTPase Rab27a. *J. Biol. Chem.* 291:25965–25982. <https://doi.org/10.1074/jbc.M116.741884>
- Jones, D.H., D.C. Anderson, B.L. Burr, H.E. Rudloff, C.W. Smith, S.S. Krater, and F.C. Schmalstieg. 1988. Quantitation of intracellular Mac-1 (CD11b/CD18) pools in human neutrophils. *J. Leukoc. Biol.* 44:535–544. <https://doi.org/10.1002/jlb.44.6.535>
- Kovács, M., J. Tóth, C. Hetényi, A. Málnási-Csizmadia, and J.R. Sellers. 2004. Mechanism of blebbistatin inhibition of myosin II. *J. Biol. Chem.* 279: 35557–35563. <https://doi.org/10.1074/jbc.M405319200>
- Kriebel, P.W., R. Majumdar, L.M. Jenkins, H. Senoo, W. Wang, S. Ammu, S. Chen, K. Narayan, M. Iijima, and C.A. Parent. 2018. Extracellular vesicles direct migration by synthesizing and releasing chemotactic signals. *J. Cell Biol.* 217:2891–2910. <https://doi.org/10.1083/jcb.201710170>
- Lai, C.P., E.Y. Kim, C.E. Badr, R. Weissleder, T.R. Mempel, B.A. Tannous, and X.O. Breakefield. 2015. Visualization and tracking of tumour extracellular vesicle delivery and RNA translation using multiplexed reporters. *Nat. Commun.* 6:7029. <https://doi.org/10.1038/ncomms8029>
- Lämmermann, T., and W. Kastenmüller. 2019. Concepts of GPCR-controlled navigation in the immune system. *Immunol. Rev.* 289:205–231. <https://doi.org/10.1111/immr.12752>
- Lämmermann, T., P.V. Afonso, B.R. Angermann, J.M. Wang, W. Kastenmüller, C.A. Parent, and R.N. Germain. 2013. Neutrophil swarms require LTB₄ and integrins at sites of cell death in vivo. *Nature.* 498: 371–375. <https://doi.org/10.1038/nature12175>
- Liew, P.X., and P. Kubes. 2019. The neutrophil's role during health and disease. *Physiol. Rev.* 99:1223–1248. <https://doi.org/10.1152/physrev.00012.2018>

- Lim, K., Y.-M. Hyun, K. Lambert-Emo, T. Capece, S. Bae, R. Miller, D.J. To-pham, and M. Kim. 2015. Neutrophil trails guide influenza-specific CD8⁺ T cells in the airways. *Science*. 349. aaa4352. <https://doi.org/10.1126/science.aaa4352>
- Luberto, C., D.F. Hassler, P. Signorelli, Y. Okamoto, H. Sawai, E. Boros, D.J. Hazen-Martin, L.M. Obeid, Y.A. Hannun, and G.K. Smith. 2002. Inhibition of tumor necrosis factor-induced cell death in MCF7 by a novel inhibitor of neutral sphingomyelinase. *J. Biol. Chem.* 277:41128–41139. <https://doi.org/10.1074/jbc.M206747200>
- Lucas-Lopez, C., S. Patterson, T. Blum, A.F. Straight, J. Toth, A.M.Z. Slawin, T.J. Mitchison, J.R. Sellers, and N.J. Westwood. 2005. Absolute stereochemical assignment and fluorescence tuning of the small molecule tool, (–)-blebbistatin. *European J. Org. Chem.* 2005:1736–1740.
- Majumdar, R., M. Sixt, and C.A. Parent. 2014. New paradigms in the establishment and maintenance of gradients during directed cell migration. *Curr. Opin. Cell Biol.* 30:33–40. <https://doi.org/10.1016/j.ceb.2014.05.010>
- Majumdar, R., A. Tavakoli Tameh, and C.A. Parent. 2016. Exosomes mediate LTB₄ release during neutrophil chemotaxis. *PLoS Biol.* 14. e1002336. <https://doi.org/10.1371/journal.pbio.1002336>
- Masedunskas, A., and R. Weigert. 2008. Intravital two-photon microscopy for studying the uptake and trafficking of fluorescently conjugated molecules in live rodents. *Traffic*. 9:1801–1810. <https://doi.org/10.1111/j.1600-0854.2008.00798.x>
- Milberg, O., A. Shitara, S. Ebrahim, A. Masedunskas, M. Tora, D.T. Tran, Y. Chen, M.A. Conti, R.S. Adelstein, K.G. Ten Hagen, et al. 2017. Concerted actions of distinct nonmuscle myosin II isoforms drive intracellular membrane remodeling in live animals. *J. Cell Biol.* 216:1925–1936. <https://doi.org/10.1083/jcb.201612126>
- Miyabe, Y., C. Miyabe, T.T. Murooka, E.Y. Kim, G.A. Newton, N.D. Kim, B. Haribabu, F.W. Luscinikas, T.R. Mempel, and A.D. Luster. 2017. Complement C5a receptor is the key initiator of neutrophil adhesion igniting immune complex-induced arthritis. *Sci. Immunol.* 2. eaaj2195. <https://doi.org/10.1126/sciimmunol.aaj2195>
- Miyabe, Y., C. Miyabe, V. Mani, T.R. Mempel, and A.D. Luster. 2019. Atypical complement receptor C5aR2 transports C5a to initiate neutrophil adhesion and inflammation. *Sci. Immunol.* 4. eaav5951. <https://doi.org/10.1126/sciimmunol.aav5951>
- Oyoshi, M.K., R. He, Y. Li, S. Mondal, J. Yoon, R. Afshar, M. Chen, D.M. Lee, H.R. Luo, A.D. Luster, et al. 2012. Leukotriene B₄-driven neutrophil recruitment to the skin is essential for allergic skin inflammation. *Immunity*. 37:747–758. <https://doi.org/10.1016/j.immuni.2012.06.018>
- Popliment, H., A. Georgantzoglou, M. Boulch, H.A. Walker, C. Coombs, F. Papaleonidopoulou, and M. Sarris. 2020. Neutrophil swarming in damaged tissue is orchestrated by connexins and cooperative calcium alarm signals. *Curr. Biol.* 30:2761–2776.e7. <https://doi.org/10.1016/j.cub.2020.05.030>
- Raposo, G., and W. Stoorvogel. 2013. Extracellular vesicles: exosomes, microvesicles, and friends. *J. Cell Biol.* 200:373–383. <https://doi.org/10.1083/jcb.201211138>
- Riedl, J., K.C. Flynn, A. Raducanu, F. Gärtner, G. Beck, M. Bösl, F. Bradke, S. Massberg, A. Aszodi, M. Sixt, et al. 2010. Lifeact mice for studying F-actin dynamics. *Nat. Methods*. 7:168–169. <https://doi.org/10.1038/nmeth0310-168>
- Rochon, Y.P., T.J. Kavanagh, and J.M. Harlan. 2000. Analysis of integrin (CD11b/CD18) movement during neutrophil adhesion and migration on endothelial cells. *J. Microsc.* 197:15–24. <https://doi.org/10.1046/j.1365-2818.2000.00645.x>
- Sadik, C.D., N.D. Kim, Y. Iwakura, and A.D. Luster. 2012. Neutrophils orchestrate their own recruitment in murine arthritis through C5aR and FcγR signaling. *Proc. Natl. Acad. Sci. USA*. 109:E3177–E3185. <https://doi.org/10.1073/pnas.1213797109>
- Schumann, M.A., P. Gardner, and T.A. Raffin. 1993. Recombinant human tumor necrosis factor alpha induces calcium oscillation and calcium-activated chloride current in human neutrophils: the role of calcium/calmodulin-dependent protein kinase. *J. Biol. Chem.* 268:2134–2140.
- Shaw, S.K., S. Ma, M.B. Kim, R.M. Rao, C.U. Hartman, R.M. Froio, L. Yang, T. Jones, Y. Liu, A. Nusrat, et al. 2004. Coordinated redistribution of leukocyte LFA-1 and endothelial cell ICAM-1 accompany neutrophil transmigration. *J. Exp. Med.* 200:1571–1580. <https://doi.org/10.1084/jem.20040965>
- Shitara, A., L. Malec, S. Ebrahim, D. Chen, C. Bleck, M.P. Hoffman, and R. Weigert. 2019. Cdc42 negatively regulates endocytosis during apical membrane maintenance in live animals. *Mol. Biol. Cell*. 30:324–332. <https://doi.org/10.1091/mbc.E18-10-0615>
- Subramanian, B.C., K. Moissoglu, and C.A. Parent. 2018. The LTB₄–BLT1 axis regulates the polarized trafficking of chemoattractant GPCRs during neutrophil chemotaxis. *J. Cell Sci.* 131. jcs217422. <https://doi.org/10.1242/jcs.217422>
- Sundt, P., M.K. Pospieszalska, L.S.-L. Cheung, K. Konstantopoulos, and K. Ley. 2011. Biomechanics of leukocyte rolling. *Biorheology*. 48:1–35. <https://doi.org/10.3233/BIR-2011-0579>
- Swamydas, M., Y. Luo, M.E. Dorf, M.S. Lionakis. 2015. Isolation of mouse neutrophils. *Curr. Protoc. Immunol.* 110:3.20.1–3.20.15.
- Tager, A.M., J.H. Dufour, K. Goodarzi, S.D. Bercury, U.H. von Andrian, and A.D. Luster. 2000. BLTR mediates leukotriene B₄-induced chemotaxis and adhesion and plays a dominant role in eosinophil accumulation in a murine model of peritonitis. *J. Exp. Med.* 192:439–446. <https://doi.org/10.1084/jem.192.3.439>
- Vicente-Manzanares, M., C.K. Choi, and A.R. Horwitz. 2009. Integrins in cell migration – the actin connection. *J. Cell Sci.* 122:199–206. <https://doi.org/10.1242/jcs.018564>
- Wculek, S.K., and I. Malanchi. 2015. Neutrophils support lung colonization of metastasis-initiating breast cancer cells. *Nature*. 528:413–417. <https://doi.org/10.1038/nature16140>
- Weigert, R., N. Porat-Shliom, and P. Amornphimoltham. 2013. Imaging cell biology in live animals: ready for prime time. *J. Cell Biol.* 201:969–979. <https://doi.org/10.1083/jcb.201212130>
- Werz, O.. 2002. 5-Lipoxygenase: cellular biology and molecular pharmacology. *Curr. Drug Targets Inflamm. Allergy*. 1:23–44. <https://doi.org/10.2174/1568010023344959>
- Xu, C., and J.L. Prince. 1998. Snakes, shapes, and gradient vector flow. *IEEE Trans. Image Process.* 7:359–369. <https://doi.org/10.1109/83.661186>
- Zarbock, A., and K. Ley. 2008. Mechanisms and consequences of neutrophil interaction with the endothelium. *Am. J. Pathol.* 172:1–7. <https://doi.org/10.2353/ajpath.2008.070502>
- Zehrer, A., R. Pick, M. Salvermoser, A. Boda, M. Miller, K. Stark, L.T. Weckbach, B. Walzog, and D. Begandt. 2018. A fundamental role of Myh9 for neutrophil migration in innate immunity. *J. Immunol.* 201:1748–1764. <https://doi.org/10.4049/jimmunol.1701400>

Supplemental material

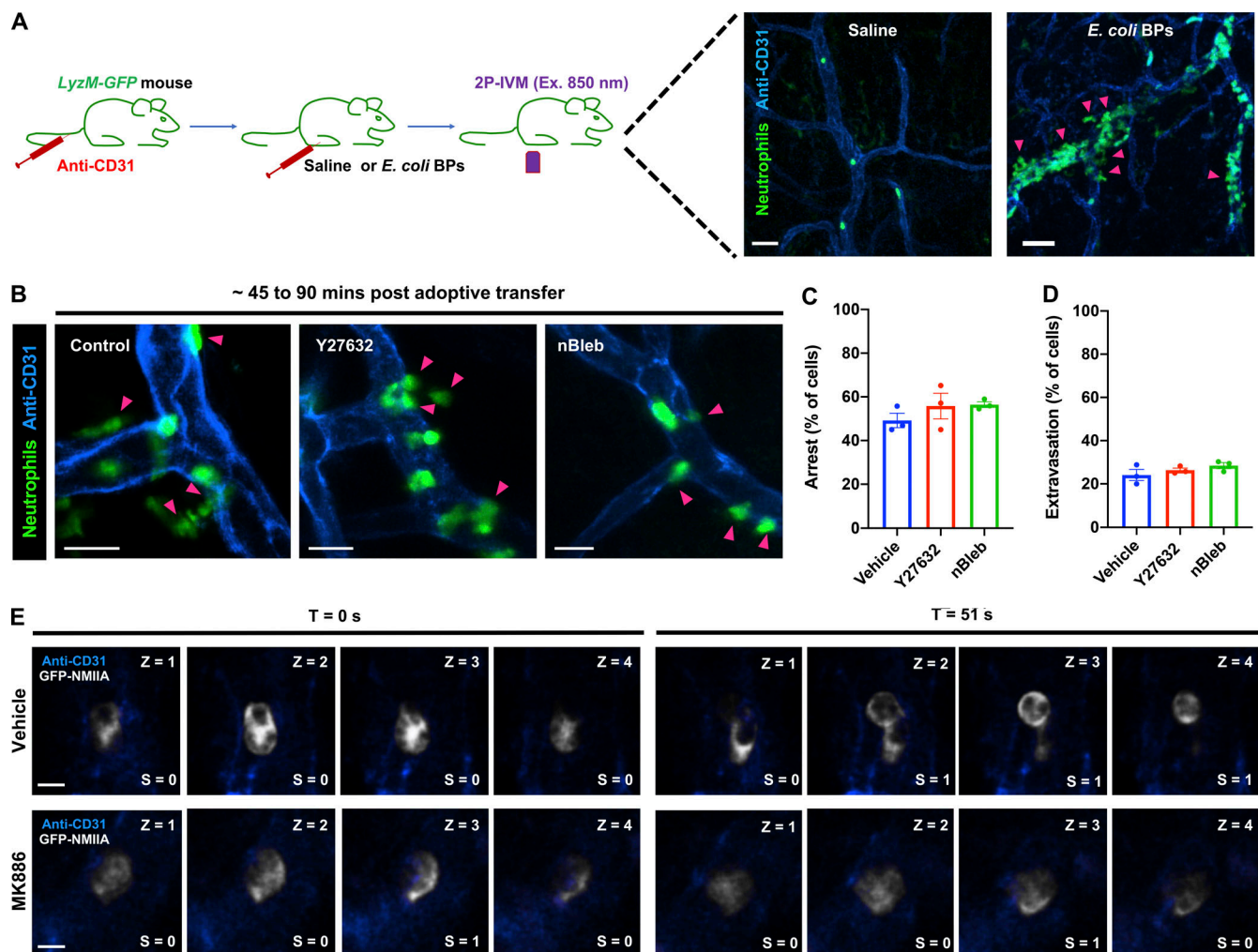


Figure S1. A sterile inflammation model in the mouse hind footpad using 2P-IVM. (A) Setup of the mouse footpad inflammation model. Upper panel: Diagram of the 2P-IVM procedure in the *LyzM-GFP* mouse footpad. Lower panels: Mice were injected with either saline (left panel) or *E. coli* BPs (right panel) in their foot pads and imaged ~40–60 min after treatment by 2P-IVM. Maximum-intensity projection of Z-stacks is presented. Vasculature is shown in blue and neutrophils in green. Pink arrowheads mark extravasating neutrophils (right panel). Scale bars = 40 μ m. The experiments were performed in $n = 2$ mice. See Video 1. (B–D) Neutrophils purified from WT mice were stained with CellTracker Green CMFDA, treated with either 40 μ M Y27632 or 10 μ M nBleb or the vehicle (DMSO) for ~30 min, adoptively transferred into *Alox5*^{-/-} mice with inflamed footpads, and imaged by 2P-IVM. Maximum-intensity projections of Z-stacks are presented (B). Magenta arrowheads highlight neutrophils (green) extravasating from the blood vessels (blue). Scale bars = 20 μ m. Quantification of the percentage of neutrophils that exhibited arrest (C) or extravasation (D) during the late phase of response, typically 45–90 min after neutrophil transfer to the recipient mice. Data are plotted as mean \pm SEM from $n = 3$ mice for each condition, and each dot represents the result from an individual animal. No significant difference was observed upon analysis with unpaired *t* test with Welch's correction. Unpaired *t* test with Welch's correction was used to determine statistical significance. (E) Neutrophils purified from *GFP-NMIIA* mice were treated with either the vehicle (DMSO; top row) or 5 μ M MK886 (bottom row), injected into *Alox5*^{-/-} mice with inflamed footpads, and imaged in time-lapse mode by ISMic. The optical sections were used to quantify the redistribution index of GFP-NMIIA. Scale bars = 3 μ m. For each time point, each section in the z axis was given a score of 0 or 1 if the GFP-NMIIA was enriched at the center or cortex, respectively, of an arrested neutrophil manually. An index was generated by averaging the score to the number of stacks analyzed for each neutrophil that displayed arrest behavior during ISMic analysis. For further details, see the Materials and methods section.

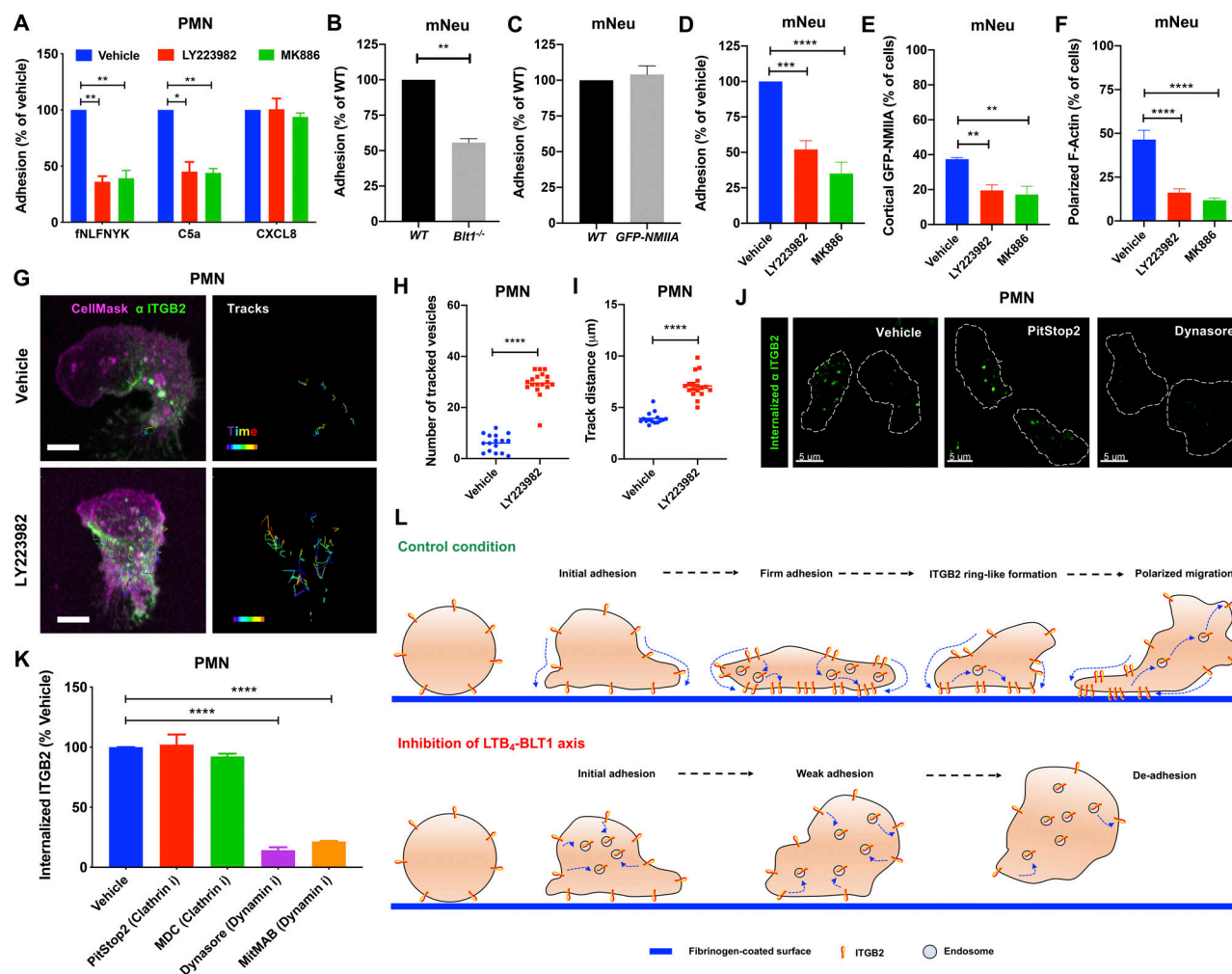


Figure S2. LTB_4 signaling promotes the adhesion of primary human and mouse neutrophils in vitro. (A) PMNs were pretreated with the vehicle or 2 μ M MK886 or 20 μ M LY223982 for 20 min and stimulated with 25 nM fNLFNYK or 250 ng/ml C5a or 250 ng/ml CXCL8 for 15 min. Adhesion was calculated as described in the Materials and Methods section and presented as a percentage relative to the respective vehicle controls for each chemoattractant. Data are plotted as mean \pm SEM from $n = 4$ independent experiments. Two-way ANOVA using Dunnett's multiple comparisons test was performed to determine statistical significance. (B and C) Neutrophils from WT (B and C), *Bltl*^{-/-} (B), and GFP-NMIIA (C) mice were stimulated with 25 nM WKYMVM for 15 min on a fibrinogen-coated surface. Adhesion was calculated as described in the Materials and Methods section and presented as a percentage relative to the WT controls. Data are plotted as mean \pm SEM from $n = 3$ independent experiments in each panel. An unpaired t test with Welch's correction was used to determine statistical significance, and no significant difference was observed between conditions in C. mNeu label stands for data from mouse primary neutrophils. (D–F) GFP-NMIIA neutrophils were pretreated with the vehicle or 2 μ M MK886 or 20 μ M LY223982 for 20 min, stimulated with 25 nM WKYMVM for 15 min, washed, fixed, and stained with rhodamine phalloidin. Adhesion was calculated as described in the Materials and Methods section and presented as a percentage of vehicle-treated controls (D). Quantification of the percentage of neutrophils exhibiting cortical NMIIA (E) and polarized F-actin (F) in response to the above-mentioned treatments. Data are plotted as mean \pm SEM from $n = 3$ independent experiments. One-way ANOVA using Dunnett's multiple comparisons test was performed to determine statistical significance. mNeu label stands for data from mouse primary neutrophils. (G–I) PMNs were pretreated with either the vehicle or 20 μ M LY223982 for 20 min. They were incubated with an Alexa Fluor 488-conjugated antibody against human ITGB2 (α ITGB2, CTB104 clone; green) in combination with CellMask Deep Red (magenta) before stimulation with 100 nM fNLFNYK for 10 min on a fibrinogen-coated surface and acquired in 3D using time-lapse mode in confocal microscopy. The trajectory of the internalized vesicles was determined as described in the Materials and Methods section (G). Tracks of individual ITGB2-containing vesicles between 5 and 7 min after stimulation are overlaid on the maximum-intensity projections derived from Z-stacks. Scale bars = 5 μ m. See Video 7. Quantification of the number (H) and distance (I) traveled by ITGB2-containing vesicles for each condition. Data are plotted for individual cells with $n = 16$ cells in vehicle and $n = 18$ cells in LY223982 treatment from $n = 3$ independent experiments. An unpaired t test with Welch's correction was used to determine statistical significance. (J and K) PMNs were pretreated for 20 min with vehicle (DMSO) or the indicated inhibitors of clathrin and dynamin (5 μ M PitStop2 or 100 μ M MDC or 50 μ M dynasore or 2.5 μ M MIMAB), stimulated for 10 min with 25 nM fNLFNYK, fixed, and imaged by confocal microscopy. Representative confocal images of PMNs with internalized ITGB2 under indicated conditions are presented (J). White dashed lines indicate cell boundary. Scale bars = 5 μ m. The extent of ITGB2 internalization was determined as described in the Materials and Methods section, and the data are plotted as the percentage change with respect to the vehicle (K). Data are represented as mean \pm SEM from $n = 3$ independent experiments. One-way ANOVA using Dunnett's multiple comparisons test was performed to determine statistical significance. (L) A model of ITGB2 trafficking regulated by the LTB_4 -BLT1 axis in PMNs. The figure depicts the progression of PMN adhesion on a fibrinogen-coated surface. In control condition, ITGB2 clusters and migrates to the bottom of the cell to form a ringlike structure, which then disassembles as the PMN begins to migrate. However, upon blockade of LTB_4 sensing via BLT1, clusters of ITGB2 rapidly internalize and fail to assemble into a ringlike structure at the bottom of the PMN, resulting possibly in the de-adhesion of PMN with time. *, $P < 0.05$; **, $P < 0.01$; ***, $P < 0.001$; ****, $P < 0.0001$.

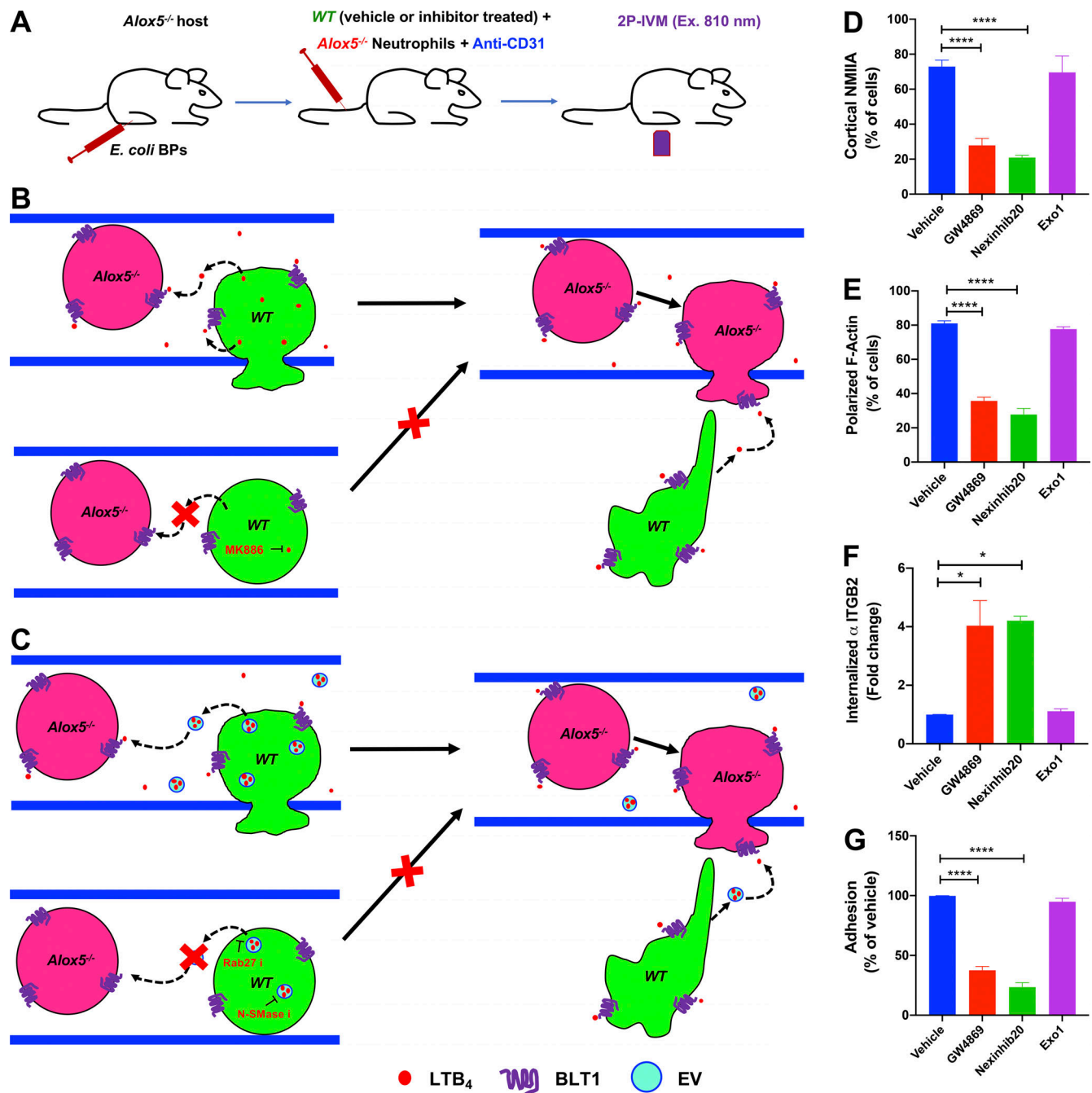


Figure S3. Inhibitors of EV pathway impair neutrophil adhesion response in vitro. (A–C) A diagram of the 2P-IVM procedure in *Alox5*^{-/-} mouse with inflamed footpad, where neutrophils from *WT* (green) were treated as indicated in Fig. 5 A for 30 min before they were coinjected with untreated *Alox5*^{-/-} neutrophils into the recipient (A). An illustration of the possible autocrine/paracrine LTB₄ signaling that occurs between *WT* and *Alox5*^{-/-} neutrophils during extravasation response when coinjected into the recipient mice with inflamed footpads and how this mechanism can be blocked using the LTB₄ inhibitor MK886 (B). An illustration of the possible EV-based autocrine/paracrine LTB₄ signaling in the conditions mentioned above that occurs in the inflamed vasculature and how this mechanism can be blocked using inhibitors of N-SMase and Rab27 (C). See Fig. 5, A and B, as well as Videos 8 and 9. **(D–G)** PMNs were pretreated for 20 min with vehicle (DMSO) or 10 μ M GW4869 or 1 μ M Nexinhib20 or 10 μ M Exo1 and stimulated in the absence or presence of α ITGB2 for 15 min with 25 nM fNLNFK, fixed, stained, and imaged by confocal microscopy. Quantification of the percentage of cells with cortical NMIIA distribution (D) and polarized F-actin (E) is presented. The extent of internalized ITGB2 (F) and cell adhesion (G) observed under the above-mentioned conditions was measured and represented as fold change and percentage with respect to vehicle control, respectively. Data are plotted as mean \pm SEM from $n = 3$ independent experiments. One-way ANOVA using Dunnett's multiple comparisons test was performed to determine statistical significance. *, $P < 0.05$; ****, $P < 0.0001$.

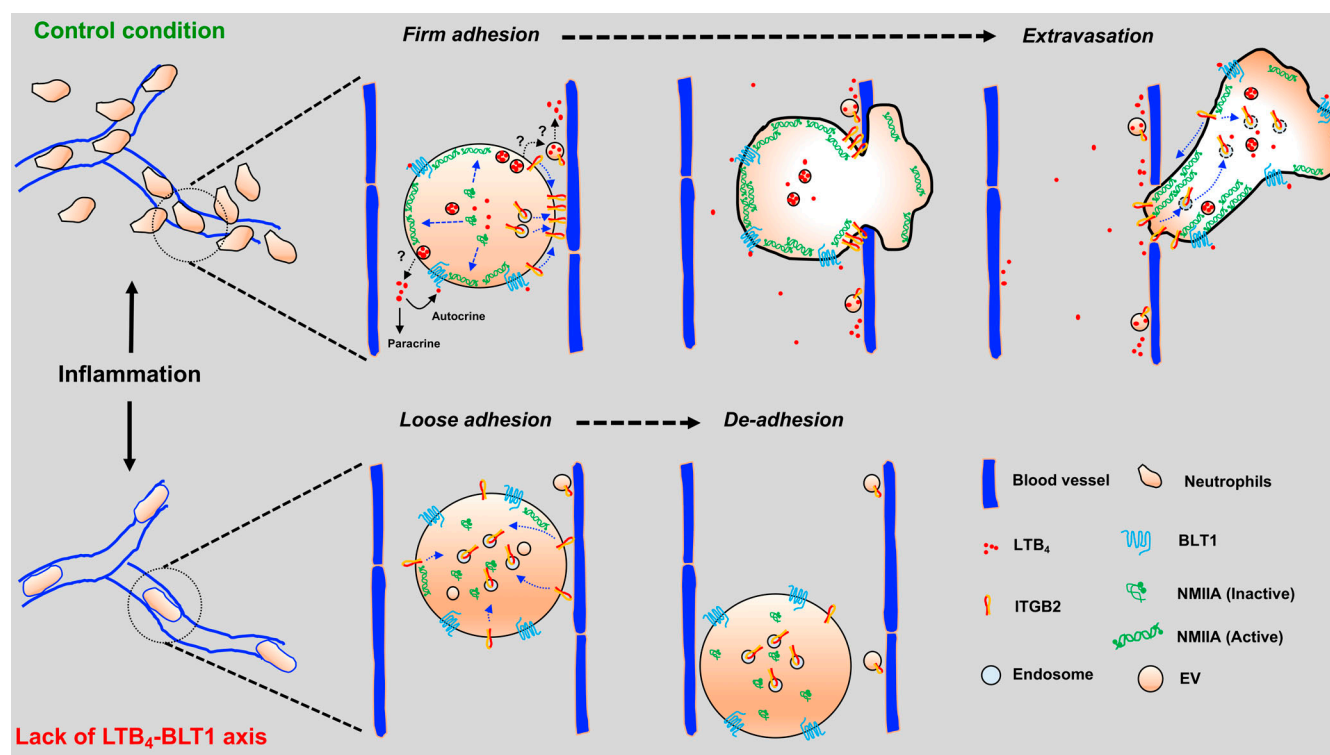


Figure S4. **Model depicting the role of the LTB_4 -BLT1 axis in promoting neutrophil arrest and extravasation in vivo.** Under control conditions, neutrophils respond to inflammatory cues by releasing EVs that relay LTB_4 signals in an autocrine/paracrine manner. The LTB_4 -BLT1 axis triggers the redistribution of NMIIA and Itgb2 for sustained arrest in the inflamed vessel, followed by extravasation into the interstitium. These mechanisms are impaired in $Alox5^{-/-}$ or $Blt1^{-/-}$ neutrophils, resulting in their reduced arrest and extravasation in response to inflammation. The specific mechanisms regulating the release of LTB_4 from EVs and the local action of LTB_4 in the inflamed vessels have yet to be determined.

Video 1. **2P-IVM of the *Lyzm-GFP* mouse footpad at ~1 h after injection of saline in one footpad and *E. coli* BPs in the other.** Videos are maximum-intensity projections of an image stack acquired for a period of ~20 min (min:s:ms) in each footpad with a frame rate of 10 frames/s. The vessels were labeled with anti-CD31 (blue). Scale bar = 50 μ m.

Video 2. **2P-IVM of the footpad in WT mouse that received labeled WT neutrophils at ~1.5 h after injection of saline in one footpad and *E. coli* BPs in the other.** Videos are maximum-intensity projections of an image stack acquired for indicated time periods (min:s:ms) in each footpad with a frame rate of 10 frames/s. The vessels were labeled with anti-CD31 (blue). Scale bar = 50 μ m.

Video 3. **2P-IVM of the inflamed *Alox5*^{-/-} mouse footpad at ~1.5 h, where labeled neutrophils (green) were introduced from WT or *Alox5*^{-/-} or *Blt1*^{-/-} mice.** Videos are maximum-intensity projections of an image stack acquired for a period of ~15–20 min (min:s:ms) for each condition with a frame rate of 10 frames/s. The vessels were labeled with anti-CD31 (blue). Scale bar = 50 μ m.

Video 4. **2P-IVM of the inflamed *Blt1*^{-/-} mouse footpad at ~1.5 h, where labeled neutrophils (green) were introduced from WT or *Alox5*^{-/-} or *Blt1*^{-/-} mice.** Videos are maximum-intensity projections of an image stack acquired for a period of ~15–20 min (min:s:ms) for each condition with a frame rate of 10 frames/s. The vessels were labeled with anti-CD31 (blue). Scale bar = 50 μ m.

Video 5. **ISMic imaging of the inflamed footpad of *Alox5*^{-/-} mouse that received either vehicle- or MK886-treated NMIIA-GFP neutrophils (white) ~1 h after inflammation.** Videos are single-slice projection from an image stack and represent ~2–4 min (min:s:ms) of acquisition for each condition with a frame rate of 5 frames/s. The vessels were labeled with anti-CD31 (blue). Scale bar = 3 μ m.

Video 6. **ISMic imaging of the inflamed footpad of *Alox5*^{-/-} mouse that received WT or *Alox5*^{-/-} neutrophils labeled for cytoplasm (CellTracker; magenta) and *Itgb2* (M18/2; white) ~1 h after inflammation.** Blood vessels are labeled with anti-CD31 (blue). Videos are maximum-intensity projections of an image stack acquired for a period of ~6–9 min (min:s:ms) of acquisition with a frame rate of 4 frames/s. Scale bar = 5 μ m.

Video 7. **Confocal imaging of ITGB2 dynamics on PMNs upon fNLFNYK stimulation in vitro. (A)** Confocal imaging of PMNs stained for PM (magenta) and α ITGB2 (white) that were pretreated with vehicle (DMSO) or BLT1 inhibitor (LY223982) for 20 min before stimulation with fNLFNYK and simultaneous live acquisition for 10 min. Videos are projections of image stacks acquired in 3D for a period of ~10 min (min:s:ms) with a frame rate of 5 frames/s. **(B)** A view of a section from the cell bottom for the conditions mentioned in A.

Video 8. **2P-IVM of the inflamed footpad at ~2 h, where labeled WT neutrophils (green) that were pretreated with vehicle (DMSO) or the inhibitors MK886 or GW4689 or Nexinhib20 or Exo1 were coinjected with labeled *Alox5*^{-/-} neutrophils (strawberry) into *Alox5*^{-/-} mice.** Videos are maximum-intensity projections of an image stack acquired for a period of ~20–22 min (min:s:ms) for each condition with a frame rate of 15 frames/s. The vessels were labeled with anti-CD31 (blue). Scale bar = 50 μ m.

Video 9. **ISMic imaging of WT neutrophils introduced into *Alox5*^{-/-} mouse with inflamed footpad ~2 h, where EVs contain CellTracker Green CMFDA (green) and *Itgb2* (M18/2 clone; red).** Videos are maximum-intensity projections of an image stack and represent ~11 min (min:s:ms) of acquisition. The vessels were labeled with anti-CD31 (cyan). Scale bar = 3 μ m. The EVs roll along and occasionally tether to the inflamed endothelial surface facing the vascular lumen in the vicinity of extravasating neutrophils.